Title
Ciliary Hedgehog Signaling Restricts Injury-Induced Adipogenesis

Journal
Cell, 170(2)

ISSN
0092-8674

Authors
Kopinke, Daniel
Roberson, Elle C
Reiter, Jeremy F

Publication Date
2017-07-01

DOI
10.1016/j.cell.2017.06.035

Peer reviewed

HHS Public Access

Author manuscript

Cell. Author manuscript; available in PMC 2018 July 13.

Published in final edited form as:

Cell. 2017 July 13; 170(2): 340–351.e12. doi:10.1016/j.cell.2017.06.035.

Ciliary Hedgehog signaling restricts injury-induced adipogenesis

Daniel Kopinke[1], **Elle C. Roberson**[1], and **Jeremy F. Reiter**[1,2]

[1]Department of Biochemistry and Biophysics, Cardiovascular Research Institute, University of California, San Francisco, San Francisco, CA, USA

SUMMARY

Injured skeletal muscle regenerates, but with age or in muscular dystrophies, muscle is replaced by fat. Upon injury, muscle-resident fibro/adipogenic progenitors (FAPs) proliferated and gave rise to adipocytes. These FAPs dynamically produced primary cilia, structures that transduce intercellular cues such as Hedgehog (Hh) signals. Genetically removing cilia from FAPs inhibited intramuscular adipogenesis, both after injury and in a mouse model of Duchenne muscular dystrophy. Blocking FAP ciliation also enhanced myofiber regeneration after injury and reduced myofiber size decline in the muscular dystrophy model. Hh signaling through FAP cilia regulated the expression of TIMP3, a secreted metalloproteinase inhibitor, that inhibited MMP14 to block adipogenesis. A pharmacological mimetic of TIMP3 blocked the conversion of FAPs into adipocytes, pointing to a strategy to combat fatty degeneration of skeletal muscle. We conclude that ciliary Hh signaling by FAPs orchestrates the regenerative response to skeletal muscle injury.

Graphical Abstract

[2]Lead author: jeremy.reiter@ucsf.edu.

SUPPLEMENTAL INFORMATION

Supplemental information includes six figures and three tables can be found with this article online at XXX.

AUTHOR CONTRIBUTIONS

D.K. conceived and executed all experiments. E.R. performed immunoblot analyses. D.K. and J.F.R. wrote the manuscript. J.F.R. supervised the study.

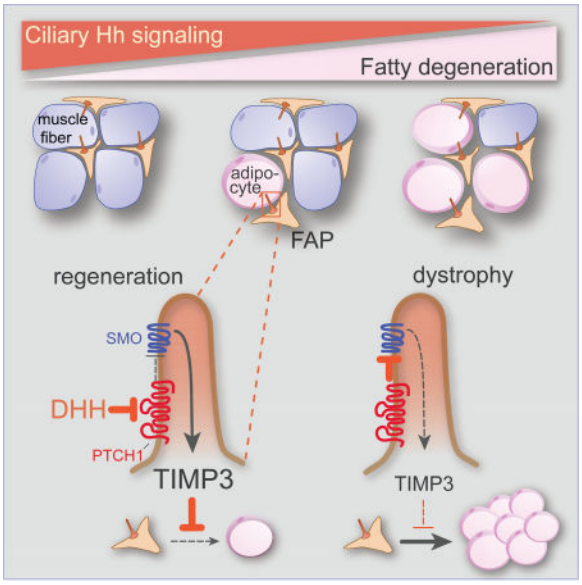

INTRODUCTION

Skeletal muscle has a high, but not inexhaustible, capacity to regenerate following injury. In chronic myopathies, such as Duchenne muscular dystrophy, fat and fibrotic scar gradually replace functional muscle, a process termed fatty degeneration (Serrano et al., 2011). Replacement of muscle by adipocytes also characterizes age-related sarcopenia and certain chronic diseases, including type 2 diabetes (Mitchell et al., 2012). How intercellular communication coordinates muscle regeneration, and how these interactions go awry to cause fatty degeneration in disease and aging, are unclear.

In addition to myogenic stem cells (MuSCs), also called satellite cells, muscle contains a second progenitor population, the non-myogenic mesenchymal cells called fibro/adipogenic progenitors (FAPs) (Joe et al., 2010; Uezumi et al., 2010). Injury induces FAPs to proliferate and promote MuSCs to form muscle (Joe et al., 2010; Uezumi et al., 2010). However, in chronic diseases, FAPs are thought to produce excess extracellular matrix (ECM) components and adipocytes, contributing to fatty degeneration (Joe et al., 2010; Lemos et al., 2015; Uezumi et al., 2011).

Many vertebrate cells possess a primary cilium, a single immotile cilium that functions in intercellular communication. During vertebrate development, primary cilia are essential for transducing Hh signals and communicating both the on and off states to the nucleus (Goetz and Anderson, 2010). In the absence of Hh signals, the cilium processes GLI transcription factors into an off state to maintain repression of Hh target genes (Hui and Angers, 2011). Upon binding of a Hh ligand [*e.g.*, Sonic hedgehog (SHH) or Desert hedgehog (DHH)] to the receptor, PTCH1, Smoothened (SMO) accumulates in the cilium to activate GLI transcription factors. Loss of cilia blocks both the formation of GLI repressor and activator, causing Hh-insensitive, low-level misexpression of Hh target genes (Liu et al., 2005; May et al., 2005).

During skeletal muscle development, Hh signaling helps to initiate the myogenic program (Hu et al., 2012). Upon muscle injury, *Shh* expression increases and may suppress fibrosis and inflammation (Straface et al., 2009). In aged mice and in a mouse model of Duchenne muscular dystrophy (DMD), forced expression of *Shh* increases MuSC proliferation, further suggesting that activating the Hh pathway in muscle may have therapeutic benefits (Piccioni et al., 2014a; Piccioni et al., 2014b).

We investigated how ciliary signaling functions in muscle regeneration. We found that the majority of ciliated cells within the muscle are FAPs which dramatically, but transiently, increase ciliation during muscle regeneration. Genetically removing cilia from FAPs protected muscle from adipogenesis following injury or upon mutation of mouse *Dystrophin* (*Dmd*), the gene mutated in DMD. Preventing FAP ciliation also enhanced myogenesis after acute injury and inhibited the loss of large muscle fibers in DMD mice. Removing cilia blocked the formation of the transcriptional repressor form of GLI3, thereby de-repressing Hh target genes. Preventing the formation of GLI3 repressor by removing PTCH1 function in FAPs or activating SMO via a small molecule agonist also blocked adipogenesis, indicating that ciliary Hh signaling controls conversion of FAPs into adipocytes. We found that ciliary signaling regulates the induction of a novel Hh downstream target, TIMP3, a secreted metalloproteinase inhibitor. TIMP3 potently inhibited adipogenesis, and treating mice with a pharmacological inhibitor of metalloproteinases prevented injury-induced adipogenesis. Thus, our results reveal that FAPs utilize ciliary Hh signaling to coordinate the regenerative response to skeletal muscle injury.

RESULTS

FAPs are dynamically ciliated during muscle regeneration

As vertebrates require cilia to interpret Hh signals, we hypothesized that ciliated cells would be involved in responding to Hh signals following injury. Therefore, we investigated which cell types are ciliated during muscle regeneration. Primary cilia were identified by staining for acetylated tubulin (TUB^{AC}) or the ciliary membrane marker ARL13B, and basal bodies were identified by staining for NINEIN or γ-TUBULIN (Figure S1A). We stained the mouse tibialis anterior muscle for ARL13B and confirmed that myofibers were not ciliated (Przybylski, 1971) (Figure S1B). MuSCs, identified by PAX7 expression, were rarely ciliated (Figure S1C). In contrast, FAPs, expressing PDGFRα, were frequently ciliated and accounted for the majority of ciliated cells within skeletal muscle (Figure 1A and Figure S1D).

To determine whether the ciliation of FAPs changes during regeneration, we utilized two distinct muscle injury models with similar regeneration kinetics. Intramuscular injection of either cardiotoxin or glycerol causes transient necrosis of muscle fibers, with cardiotoxin inducing minimal adipogenesis and glycerol inducing more (Pisani et al., 2010). We injected cardiotoxin or glycerol into tibialis anterior muscles of 10–12 week old wild type mice and analyzed the number and ciliation of FAPs at different time points post injury. As previously described (Lemos et al., 2015), muscle injury transiently increased the number of FAPs (Figure 1A and B). Intriguingly, the proportion of FAPs with cilia also increased sharply, regardless of injury type, from 10% to almost 50% before returning to pre-injury levels at 21

days post injury (dpi) (Figure 1A and 1C). Thus, a portion of FAPs are ciliated prior to an injury and FAP ciliation sharply increases during muscle repair, raising the possibility that FAPs and cilia participate in regeneration.

FAP cilia control injury-induced adipogenesis

As PDGFRα is uniquely expressed by FAPs within the muscle (Figure 1A and Figure 2A), we used a tamoxifen-inducible *Pdgfra*-CreERT allele to genetically manipulate FAPs in vivo. To validate the specificity of recombination, we generated *Pdgfra*-CreERT *Rosa26*^{EYFP} mice, which express EYFP in PDGFRα-expressing cells and their progeny upon administration of tamoxifen (Figure 2A). Both before injury and 7 dpi with cardiotoxin injection, the majority of FAPs of tamoxifen-treated *Pdgfra*-CreERT *Rosa26*^{EYFP} mice expressed EYFP (Figure 2A). Lineage tracing of FAPs using *Pdgfra*-CreERT *Rosa26*^{EYFP} mice demonstrated that the majority of PERILIPIN-expressing adipocytes induced after injury with glycerol also expressed EYFP (Figure 2A), indicating that FAPs are the major source of injury-induced adipocytes in skeletal muscle.

To assess whether FAP cilia function in muscle regeneration, we conditionally deleted *Ift88*, a gene required for ciliogenesis and ciliary maintenance, in FAPs of adult mice using *Pdgfra*-CreERT. Tamoxifen treatment recombined *Ift88* and caused a near complete loss of FAP cilia (Figure S2A). *Pdgfra*-CreERT *Ift88*$^{c/-}$ mice to which we administered tamoxifen are referred to hereafter as FAP$^{no\ cilia}$ mice. Tamoxifen-treated littermates of FAP$^{no\ cilia}$ mice that lacked either the *Pdgfra*-CreERT or possessed a wild type *Ift88* allele served as controls (Figure S2B). RT-qPCR analysis revealed that expression of *Ift88* did not recover in FAP$^{no\ cilia}$ muscle over the period we observed muscle regeneration (Figure S2C).

We used FAP$^{no\ cilia}$ mice to assess the function of FAP cilia. Loss of FAP cilia strongly impacted adipogenesis (Figure 2B). Following glycerol-induced injury, control mice, regardless of sex, exhibited extensive infiltration of PERILIPIN- and Fatty acid binding protein 4 (FABP4)-expressing adipocytes throughout the muscle (Figure 2B and Figure S2B). In contrast, FAP$^{no\ cilia}$ mice displayed an over 70% reduction in the number of adipocytes, both 7 and 21 dpi (Figure 2B and C). The adipocytes in FAP$^{no\ cilia}$ mice were of comparable size to those of control mice, suggesting that loss of FAP cilia affected adipogenesis, not maturation (Figure S2D). Although cardiotoxin induced fewer adipocytes in control mice, FAP$^{no\ cilia}$ mice injured with cardiotoxin also displayed decreased adipogenesis 21 dpi (Figure S2E).

We confirmed the difference in adipogenesis by comparing the expression levels of mature adipocyte markers such as *Adiponectin* (*Adipoq*) and *Fapb4* in whole muscle RNA lysates in an independent cohort of mice. Glycerol injury induced *Adipoq* and *Fabp4* expression in control but not in FAP$^{no\ cilia}$ mice (Figure 2D). Thus, FAP cilia control adipogenesis following muscle injury.

FAP cilia regulate intramuscular adipogenesis in a model of Duchenne muscular dystrophy

DMD is a severe human myopathy in which mutations in the *DMD* gene encoding DYSTROPHIN cause progressive myofiber death, fibrosis and replacement of myofibers with adipocytes (Hoffman et al., 1987). Mouse *Dmd*^{mdx} mutants develop a myopathy

associated with intramuscular adipogenesis (Bulfield et al., 1984). Indeed, PERILIPIN-expressing adipocytes were five times more abundant in muscle of 12 month old *Dmd*^{mdx} mice than wild type mice (Figure 3A and 3B).

As removing cilia from FAPs reduced adipogenesis following acute muscle injury, we hypothesized that removing FAP cilia may also suppress adipogenesis in a model of DMD. Therefore, we generated *Dmd*^{mdx} mice with and without FAP cilia (*Dmd*^{mdx} control and *Dmd*^{mdx} FAP$^{\text{no cilia}}$, respectively) (Figure S3A).

Recombination of the *Ift88* allele in *Dmd*^{mdx} mice was induced by administrating tamoxifen at 4 weeks of age. As intramuscular fat formation increases with age in *Dmd*^{mdx} mice, we waited one year after tamoxifen administration before assessing the effects of loss of FAP cilia on adipogenesis. To test for the removal of cilia, we quantified whether FAPs were ciliated one year after inducing recombination. Compared to FAPs of *Dmd*^{mdx} control mice, FAP ciliation was reduced by over 85% in *Dmd*^{mdx} FAP$^{\text{no cilia}}$ mice (Figure S3B). Thus, FAPs lacking cilia are present even one year after cilia deletion. In addition, ciliated FAPs did not replace FAPs that cannot generate cilia.

We assessed adipocyte formation in the tibialis anterior muscle of *Dmd*^{mdx} control and *Dmd*^{mdx} FAP$^{\text{no cilia}}$ mice. *Dmd*^{mdx} control mice displayed an increase in intramuscular fat formation compared to wild type mice (Figure 3B and S3A). Notably, removal of FAP cilia reduced the prevalence of adipocytes in *Dmd*^{mdx} mice (Figure 3A and 3B). Thus, as in the setting of acute injury, FAP cilia promote muscle adipogenesis in a model of DMD.

Removing cilia from FAPs enhances myogenesis and increases myofiber size

In *Dmd*^{mdx} mice, myofiber size decreases with age (McDonald et al., 2015). As FAPs influence myogenesis (Joe et al., 2010), we investigated whether removal of primary cilia from FAPs of *Dmd*^{mdx} mice affects myofiber size. Quantification of myofiber cross sectional area revealed that wild type myofiber size decreased with age, and this reduction was exaggerated in *Dmd*^{mdx} mice (Figure 3C–3E, S3C). Myofibers of one year old *Dmd*^{mdx} FAP$^{\text{no cilia}}$ mice were larger than those of *Dmd*^{mdx} control mice, and similar to those of 112 week old wild type mice (Figure 3C–3E). To understand whether loss of FAP cilia decreased degeneration or increased regeneration, we analyzed the frequency of myofibers with centrally located nuclei, a proxy for regenerating fibers (McDonald et al., 2015). Compared to *Dmd*^{mdx} mice, *Dmd*^{mdx} FAP$^{\text{no cilia}}$ mice displayed increased proportions of myofibers with centrally located nuclei, suggestive of enhanced myofiber repair (Figure S3D). Thus, in addition to reducing adipogenesis, removal of FAP cilia in *Dmd*^{mdx} mice was associated with increased myofiber size.

To determine whether the effect of loss of FAP cilia also affects muscle regeneration after acute injury, we analyzed myofiber size 21 days after glycerol injury. Compared to control mice, FAP$^{\text{no cilia}}$ mice exhibited increased myofiber cross sectional area following injury (Figure S3E).

To test whether the increased fiber size following injury in FAP$^{\text{no cilia}}$ mice was associated with changes in muscle regeneration, we assessed the expression of embryonic myosin

(embryonic myosin heavy chain 3, MYH3) 5 and 7 days post glycerol injury. Transient re-expression of MYH3 is a hallmark of newly formed myofibers (d'Albis et al., 1988). $FAP^{no\ cilia}$ mice produced more than threefold more MYH3-expressing myofibers than control mice 5 dpi (Figure S3F). In control mice, the prevalence of MYH3-expressing myofibers increased from 5 days to 7 days post glycerol injury (Figure S3F). In contrast, in $FAP^{no\ cilia}$ mice more MYH3-expressing myofibers are present at 5 than 7 dpi (Figure S3F). Thus, FAP cilia affect myofiber size and the extent and timing of MYH3 expression following injury, suggesting that cilia act within FAPs to restrain regeneration of myofibers.

Cilia repress FAP expression of Hh target genes

In vertebrates, primary cilia participate in Hh signal transduction by both activating GLI transcription factors and generating the GLI transcriptional repressors that repress Hh target genes in the absence of Hh signals (Hui and Angers, 2011). To assess whether primary cilia control the expression of Hh target genes in FAPs, we evaluated the expression of the Hh target genes, *Gli1* and *Ptch1*. RT-qPCR analysis of whole muscle 5 dpi with glycerol injection revealed that removing IFT88 from FAPs increased *Gli1* and *Ptch1* expression (Figure 4A). To test which cells induced *Gli1* and *Ptch1*, we examined the activity of *Ptch1-lacZ*, a reporter of Hh signaling (Goodrich et al., 1997). Both before and 5 days after glycerol injury, we detected no *Ptch1-lacZ* activity in myofibers (Figures S4A).

To assess whether the detected increase in Hh target gene expression occurred in FAPs, we purified control FAPs and FAPs lacking IFT88 from regenerating muscle using magnetic-activated cell sorting (MACS). 3dpi with glycerol injection, we isolated FAPs from dissociated tibialis anterior muscle using combined negative and positive MACS. The purified FAPs were highly enriched for PDGFRα expression, a FAP marker (Figure S4B). As with whole muscle, RT-qPCR analysis revealed that removal of IFT88 in FAPs 3 dpi with glycerol increased *Gli1* and *Ptch1* expression (Figure 4B). Thus, removing cilia from FAPs increases the expression of Hh target genes.

In the developing limb bud, primary cilia inhibit *Gli1* and *Ptch1* expression by promoting GLI3 repressor formation (Liu et al., 2005; May et al., 2005). To test whether cilia function similarly in FAPs, we assessed GLI3 repressor formation in purified FAPs 3 dpi with glycerol injection. We found that IFT88 is required for FAPs to process GLI3 into the repressor, consistent with the possibility that the elevated expression of Hh target genes in FAPs lacking cilia is due to de-repression secondary to loss of GLI3 repressor (Figure 4C).

We hypothesized that the up regulation of Hh target gene expression caused by loss of cilia inhibited adipogenesis. To test this hypothesis, we assessed whether activating Hh signal transduction in FAPs was sufficient to block injury-induced adipogenesis. PTCH1 represses the Hh pathway, and deletion of *Ptch1* causes constitutive Hh pathway activation (Goodrich et al., 1997). Therefore, we generated *Pdgfra-CreERT* $Ptch1^{c/c}$ mice (referred hereafter to as $FAP^{no\ PTCH1}$ mice) to, upon tamoxifen administration, remove *Ptch1* and activate the Hh pathway specifically in FAPs. Littermates lacking either *Pdgfra-Cre*ERT or possessing a wild type allele of *Ptch1* served as controls (Figure S4C). RT-qPCR 5 dpi with glycerol injection indicated that deletion of *Ptch1* in FAPs induced *Gli1* expression (Figure S4D).

FAP$^{no\ PTCH1}$ mice displayed an almost complete block in the generation of adipocytes 7 dpi with glycerol injection (Figure 4D and S4C). As an independent assessment, we compared the expression levels of the adipocyte markers *Adipoq* and *Perilipin* in control and FAP$^{no\ PTCH1}$ mice 5 dpi with glycerol injection. Injury did not induce these adipocyte markers specifically in FAP$^{no\ PTCH1}$ mice (Figure S4E).

As an alternative means of activating Hh signaling, we injected a small molecule Smoothened agonist (SAG) 0, 2 and 4 dpi with glycerol (Chen et al., 2002). SAG reduced adipogenesis by half at 7 dpi relative to DMSO vehicle control (Figure 4E). Thus, activating Hh signaling in FAPs, like removing cilia, strongly inhibits injury-induced intramuscular adipogenesis, suggesting that FAP cilia promote adipogenesis by restraining Hh target gene expression.

Glycerol injection produces a more potent adipogenic injury than does cardiotoxin injection. Consistent with this observation, RT-qPCR analysis of the expression of the adipocyte master regulator, *Peroxisome proliferator-activated receptor γ* (*Pparγ*) in whole tibialis anterior muscle revealed that, whereas both injuries induce *Pparγ*, only glycerol injection caused sustained induction of *Pparγ* (Figure 4F).

Given that Hh signaling represses injury-associated adipogenesis, we hypothesized that cardiotoxin, which is weakly adipogenic, activates Hh signaling more than glycerol. Assessing *Gli1* and *Ptch1* expression by RT-qPCR indicated that cardiotoxin injection induces Hh signaling at 3 and 5 dpi, but glycerol injection does not (Figure 4G). To examine whether cardiotoxin activates Hh signaling through a Hh ligand, we investigated its ability to induce *Shh*, *Ihh* or *Dhh*. RT-qPCR analysis indicated that cardiotoxin, but not glycerol, induced the expression of *Dhh* (Figure 4H). Immunofluorescent staining revealed that Schwann cells within the muscle express DHH (Figure 4I), as previously reported (Renault et al., 2013). Thus, injury with cardiotoxin, but not glycerol, induces DHH expression, activating Hh signaling.

Cilia promote FAP differentiation into adipocytes

As Hh signaling can promote proliferation, inhibit cell death, or direct differentiation, we tested the possibility that cilia inhibit adipogenesis through effects on FAP proliferation, cell death or differentiation. To determine whether cilia affect the proliferation of FAPs following injury, we injured FAP$^{no\ cilia}$ mice and quantified PDGFRα-expressing FAPs. During the initial 5 dpi, removing IFT88 from FAPs did not affect the number of intramuscular FAPs (Figure S5A). To further assess whether cilia affect FAP proliferation, we administered BrdU to FAP$^{no\ cilia}$ and control mice either two hours prior to tissue harvesting at the indicated time points post-injury (Figure S5B) or repeatedly over the first two days post injury (Figure S5C). Loss of IFT88 caused no significant difference in the proliferation index of FAPs, further supporting the conclusion that cilia do not restrain adipogenesis through effects on FAP expansion (Figure S5B and C).

To determine whether FAP cilia inhibit apoptosis, we measured the proportion of FAPs positive for cleaved CASPASE3, a marker of apoptosis, in control and FAP$^{no\ cilia}$ mice

(Figure S5D). Removal of IFT88 did not affect apoptosis, indicating that alterations in cell survival also do not account for cilium-dependent effects on adipogenesis.

To test the idea that FAP cilia regulate adipocyte differentiation, we examined the induction of transcription factors of the CCAAT/enhancer-binding protein family (C/EBPα and C/EBPβ) and PPARγ, regulators of early adipocyte differentiation. We used MACS to isolate FAPs from control and $FAP^{no\ cilia}$ muscle 3 dpi with glycerol injection, a time before mature adipocytes have formed. RT-qPCR analysis of these FAPs demonstrated that IFT88 is required for the full induction of *C/ebpα*, *C/ebpβ* and *Pparγ*, suggesting that cilia are critical for an early step in adipocyte differentiation (Figure 5A).

FAP cilia restrict adipogenesis through a cell non-autonomous mechanism

In neural and limb bud patterning, ciliary Hh signaling is thought to act cell autonomously to direct differentiation. To address whether cilia affect FAP differentiation cell autonomously, we generated *Pdgfra-CreERT Ift88*$^{c/-}$ *Rosa26*^{EYFP} mice (referred to here as $FAP^{lineage\ +\ no\ cilia}$) to remove IFT88 and indelibly mark FAPs and their descendants with EYFP (Figure 5B). EYFP-expressing FAPs of $FAP^{lineage\ +\ no\ cilia}$ mice exhibited an 85% reduction in ciliation (Figure S5E and F). Removing cilia did not affect the number of EYFP-expressing FAPs after injury, further indicating that FAP cilia do not affect proliferation or cell death (Figure S5G).

To assess whether cilia affect adipogenesis cell autonomously or non-autonomously, we induced recombination in a subset of FAPs (Figure 5B). If cilia restrict adipogenesis cell autonomously, we reasoned that EYFP-marked FAPs without cilia should give rise to fewer adipocytes than do EYFP-negative FAPs that retain cilia. If FAP cilia act cell non-autonomously, the number of both EYFP-positive and EYFP-negative adipocytes should be reduced following deletion of cilia in the EYFP-marked FAPs.

Following a moderate dose of tamoxifen, approximately 60% of adipocytes in control mice expressed EYFP at 21 dpi (Figure 5C and D). The proportion of adipocytes expressing EYFP in $FAP^{lineage\ +\ no\ cilia}$ mice was the same as that of $FAP^{lineage}$ mice at both 5 and 21 dpi (Figure 5C and D). Thus, loss of cilia in a fraction of FAPs affects adipocyte differentiation by both those FAPs that express IFT88 and those that do not, indicating that the cilia of FAPs restrict adipogenesis cell non-autonomously.

To assess whether FAP cilia also function cell non-autonomously to restrict adipogenesis in *Dmd*^{mdx} mice, we generated *Dmd*^{mdx} *Pdgfra-CreERT Ift88*$^{c/-}$ *Rosa26*^{EYFP} mice (referred to hereafter as *Dmd*^{mdx} $FAP^{lineage\ +\ no\ cilia}$ mice). Similar to the acute injury model, the proportion of adipocytes that expressed EYFP was equivalent in *Dmd*^{mdx} $FAP^{lineage}$ control and *Dmd*^{mdx} $FAP^{lineage\ +\ no\ cilia}$ mice (Figure S5H and I). Therefore, the cilia of FAPs promote adipogenesis cell non-autonomously in both acute injury and chronic degeneration. As cell non-autonomous effects are often mediated via secreted signals, we investigated whether ciliary Hh signaling controlled the production of a secreted inhibitor of adipogenesis.

Ciliary Hedgehog signaling induces TIMP3, an inhibitor of adipocyte formation

Soon after injury (3 dpi), FAP$^{no\ cilia}$ mice showed reduced induction of the early adipocyte regulators *C/ebpα*, *C/ebpβ* and *Pparγ* (Figure 5C). To more fully understand the cilium-dependent regulation of injury-induced adipogenesis, we used RNA-seq to transcriptionally profile FAPs purified by MACS from control or FAP$^{no\ cilia}$ mice 3 dpi with glycerol injection (Figure 6A). We identified 609 differentially expressed genes affected by loss of IFT88 (Table S1). As activation of Hh signaling is able, like loss of cilia, to suppress adipogenesis, we compared cilia-dependent genes to previously identified Hh target genes (see Supplemental methods). Three de-repressed genes identified by this analysis were *Ptch1, Gli1*, both established general targets of Hh signaling, and *Timp3* (Figure S6A). *Timp3* encodes Tissue inhibitor of metalloproteinase 3, a secreted inhibitor of members of the matrix metalloproteinase (MMP) and "a disintegrin and metalloproteinase" (ADAM) families (Khokha et al., 2013). RT-qPCR analysis of independent samples of purified FAPs from control and FAP$^{no\ cilia}$ mice confirmed that loss of FAP cilia increased expression of *Timp3* (Figure 6B).

As our data had indicated that both removal of cilia and removal of PTCH1 from FAPs blocks injury-induced adipogenesis, we examined whether, like loss of cilia, loss of PTCH1 increases *Timp3* expression. RT-qPCR analysis of whole muscle of FAP$^{no\ PTCH1}$ and control mice demonstrated that removing PTCH1 from FAPs also up regulates *Timp3* expression (Figure S6B). As addition of TIMP3 to 3T3-L1 cells, a commonly used model of adipogenesis, had previously been shown to inhibit adipogenesis in vitro (Bernot et al., 2010), we hypothesized that elevated *Timp3* expression by FAPs may underlie the cell non-autonomous suppression of adipogenesis caused by loss of cilia in vivo. Examination of ciliogenesis during 3T3-L1 adipogenesis revealed that nearly all 3T3-L1 cells possessed cilia prior to differentiation, but lost their cilia as they differentiated into adipocytes (Figure S6C), similar to previous reports (Marion et al., 2009; Zhu et al., 2009) and like FAPs in vivo (Figure S2A). Hh signaling had previously been shown to inhibit 3T3-L1 adipogenesis (Pospisilik et al., 2010; Suh et al., 2006). We confirmed that activating Hh signaling with SAG inhibited 3T3-L1 differentiation into adipocytes: SAG induced expression of *Gli1* and *Ptch1* in a dose dependent fashion, suppressed adipogenesis at low concentration (3 nM), and blocked adipogenesis at high concentration (100 nM) (Figure 6C and D). Concordantly, SAG inhibited the induction of adipocyte genes such as *Pparγ*, *Adipoq* and *Perilipin* (Figure S6E).

To test whether the Hh pathway regulates *Timp3* expression in 3T3-L1 cells, as it does in FAPs, we stimulated 3T3-L1 cells with SAG and assessed *Timp3* expression by RT-qPCR. Activating Hh signaling potently induced *Timp3* expression (Figure S6F).

If Hh signaling suppresses adipogenesis through induction of *Timp3*, we reasoned that inhibition of *Timp3* expression should block the suppressive effects of SAG in 3T3-L1 cells. To test this hypothesis, we used siRNAs to suppress *Timp3* expression (Figure S6F). Suppressing *Timp3* expression blocked the ability of low SAG and reduced the ability of high SAG concentration to inhibit adipogenesis (Figure 6C and D). Similarly, knockdown of *Timp3* blocked (in the case of low SAG) or reduced (in the case of high SAG) the repressive effect of Hh signaling on the expression of the adipocyte genes *Pparγ, Adipoq* and *Perilipin*

(Figure S6E). Thus, in 3T3-L1 cells, Hh signaling acts through TIMP3, directly or indirectly, to repress adipogenesis.

MMP14 promotes adipogenesis downstream of or in parallel to TIMP3

Adipogenesis involves the remodeling of the ECM by matrix metalloproteinases (MMPs) (Mariman and Wang, 2010). If TIMP3 suppresses adipogenesis by inhibiting an MMP, inhibition of that MMP would also suppress adipogenesis. To identify MMPs that TIMP3 may inhibit in adipogenesis, we analyzed the RNA-seq data and identified two expressed MMPs that promote adipogenesis, MMP2 and MMP14 (also called MT1-MMP) (Bauters et al., 2015; Chun et al., 2006), and two not recognized to affect adipogenesis, MMP16 and MMP23. To test for possible roles in promoting adipogenesis, we transfected 3T3-L1 cells with siRNA against MMP16 or MMP23 four days prior to induction, or treated cells with a pharmacologic inhibitor of MMP2 (MMP-2 Inhibitor II) at the day of induction. Inhibiting MMP2 or MMP16 function had no effect on adipogenesis, and inhibition of MMP23 induced cell death (Figure S6G), suggesting that these MMPs do not mediate the effects of TIMP3.

To assess MMP14 function, we used siRNA to inhibit 3T3-L1 expression of *Mmp14* four days before induction of adipogenesis. RT-qPCR confirmed inhibition of *Mmp14* expression (Figure S6H). Inhibiting *Mmp14* inhibited adipogenesis (Figure 6E and 6F). As independent test of the effect of MMP14 on adipogenesis, we tested whether inhibiting *Mmp14* affected expression of the adipocyte genes *Adipoq, Perilipin* and *Pparγ* by RT-qPCR 3 days post induction of adipogenesis. Like removing cilia from FAPs, inhibiting *Mmp14* repressed induction of these adipocyte genes (Figure S6I).

As TIMP3 inhibits MMP14 (Wei et al., 2005) and MMP14 promotes adipogenesis (Chun et al., 2006), we inhibited both to assess whether MMP14 may act downstream of TIMP3. Using siRNA-mediated knockdown, we depleted *Timp3* and *Mmp14* in 3T3-L1 cells singly or in combination. Inhibiting both *Timp3* and *Mmp14* impaired adipogenesis demonstrating that inhibiting *Timp3* could not restore adipogenesis in the absence of MMP14 function (Figure 6E and 6F). The lack of rescue was confirmed by RT-qPCR for the adipogenic markers *Adipoq*, *Perilipin* and *Pparγ* (Figure S6I).

To further test whether MMP14 participates in adipogenesis, we treated 3T3-L1 cells with NSC405020, an MMP14-specific inhibitor. NSC405020 potently inhibited formation of adipocytes (Figures S6J). RT-qPCR analysis revealed that NSC405020 also repressed induction of the adipocyte genes *Adipoq*, *Perilipin* and *Pparγ* (Figure S6I). SiRNA-mediated depletion of *Timp3* did not restore adipogenesis to NSC405020 treated 3T3-L1 cells (Figures S6I and S6J), consistent with an effect of MMP14 downstream of or in parallel to TIMP3 (Figure 6G). Thus, we propose that ciliary Hh signaling induces TIMP3 to restrict MMP14 activity, thereby inhibiting adipogenesis.

A pharmacological mimetic of TIMP3 inhibits intramuscular adipogenesis in vivo

As TIMP3 inhibits adipogenesis in vitro, we investigated whether TIMP3 may also inhibit adipogenesis in vivo. Cardiotoxin injection was marked by a transient decline in *Timp3* expression, whereas glycerol injection, a more adipogenic injury, caused a sustained

suppression of *Timp3* expression, consistent with a role for TIMP3 in inhibiting adipogenesis (Figure 7A). To assess whether down regulation of TIMP3 activity promotes adipogenesis, we tested whether maintaining TIMP3-like activity can inhibit intramuscular adipogenesis. To mimic the activity of TIMP3, we made use of batimastat, a pharmacological inhibitor of metalloproteinases including MMP14 (Hotary et al., 2002; Macaulay et al., 1999). We confirmed that batimastat inhibited 3T3-L1 cell adipogenesis (Chavey et al., 2003) (Figure 7B).

Given its ability to inhibit adipogenesis in vitro, we assessed whether batimastat prevents injury-induced adipogenesis in vivo. Wild type mice were injected with batimastat at the day of injury by glycerol injection (day 0) and at 2 dpi. By 7 dpi, batimastat reduced adipocyte number within skeletal muscle by 70% (Figure 7C). Thus, a small molecule mimetic of TIMP3 suppresses injury-induced muscle adipogenesis, revealing a pharmacological approach for blocking the mechanism by which cilia-mediated Hh signaling promotes fat formation.

DISCUSSION

Replacement of muscle with fat is a sequla of both age and diverse chronic diseases. FAPs give rise to adipocytes following injury and this conversion is regulated by Hh signaling through the primary cilium. Removing cilia from FAPs not only reduces intramuscular adipogenesis, but also enhanced hallmarks of muscle healing. A Hh regulated secreted factor, TIMP3, inhibits MMP14 and restrains adipogenesis, pointing to a strategy for reducing fatty degeneration and improving the regeneration of skeletal muscle following injury.

In vertebrates, cilia are present on most cell types. To explore the post-developmental functions of cilia in skeletal muscle, we identified which muscle cell types are ciliated and found that, consistent with previous reports (Marion et al., 2009; Przybylski, 1971; Zhu et al., 2009), mature muscle fibers and adipocytes are not ciliated. Nonetheless, skeletal muscle contains many ciliated cells, most of which are FAPs.

Intriguingly, FAPs not only increase in numbers but also in their ciliation during the early phases of regeneration. Thus, cilia are present at a time and place to control FAP fate. Genetic manipulation revealed that cilia promote the conversion of FAPs into adipocytes following injury. Similarly, in a model of Duchenne muscular dystrophy, cilia also promote the adipogenic conversion of FAPs, indicating that cilia influence adipogenesis both acutely following injury and in a chronic disease model.

One of the most well characterized functions of vertebrate cilia is the transduction of Hh signals. Similar to limb bud development, removal of FAP cilia diminished formation of GLI3 repressor and depressed Hh target genes, indicating that ciliary Hh signaling can function similarly during development and tissue regeneration.

Like removal of cilia, activating Hh signaling in FAPs by conditionally deleting *Ptch1* or administering SAG blocked injury-induced adipogenesis. Our finding that Hh signaling restrains intramuscular adipogenesis parallels previously identified roles for Hh signaling in

suppressing adipocyte differentiation in vitro and during development (Pospisilik et al., 2010; Suh et al., 2006), underlining the importance of Hh signals in restricting adipogenesis in diverse settings.

Mesenchymal cell populations similar to FAPs exist in tissues beyond skeletal muscle, and in many of these tissues, ectopic fat formation is a consequence of chronic diseases (Montani et al., 2004; Pinnick et al., 2008). The cells that give rise to fat in these tissues and the signals involved, however, are unknown. As a subset of mesenchymal cells in diverse tissues expresses the Hh target gene, *Gli1* (Kramann et al., 2015), we hypothesize that ciliary Hh signaling in these cells regulates fibrosis or adipogenesis through mechanisms similar to those employed by FAPs.

While overexpression of SHH can affect muscle regeneration (Piccioni et al., 2014a; Piccioni et al., 2014b), it has not been clear whether injury induces an endogenous Hh signal. Schwann cells robustly expressed DHH upon cardiotoxin injury, but not glycerol injury, and cardiotoxin injury, but not glycerol injury, activated the Hh pathway. Because pharmacologically activating the Hh pathway, like cardiotoxin injury, suppressed adipogenesis, the induction of DHH may account for why cardiotoxin injury causes limited adipogenesis.

In other tissues, Hh signals from nerves control target cell behaviors (Brownell et al., 2011). Intriguingly, denervating muscle causes intramuscular adipogenesis (Dulor et al., 1998). It will be interesting to test whether diminished production of DHH by Schwann cells causes increased FAP conversion into adipocytes upon denervation.

Activation of the Hh pathway after injury diminishes with age or loss of Dystrophin in mice, correlating with increased intramuscular adipogenesis (Piccioni et al., 2014a; Piccioni et al., 2014b). The inverse correlation between Hh pathway activation and adipogenesis raises the possibility that the deregulation of Hh signaling is a key determinant of age-associated FAP-mediated adipogenesis.

In FAPs, mosaic removal of cilia combined with fate mapping indicates that cilia act cell non-autonomously to block adipogenesis, although we cannot exclude a partially cell autonomous effect. These results suggest that, in response to injury, FAPs expand and then communicate with each other to coordinate their fate. To determine how cilia cell non-autonomously repress adipogenesis, we compared the transcriptomes of control FAPs and FAPs from which we had genetically removed cilia. We identified that ciliary Hh signaling in FAPs regulates expression of *Timp3*. Future experiments will determine whether *Timp3* is a direct or indirect target of Hh signaling.

Timp3 encodes a secreted inhibitor of several MMPs and ADAM proteins, overexpression of which reduces adipogenesis (Bernot et al., 2010; Khokha et al., 2013). Suppressing *Timp3* expression blocked the ability of Hh pathway activation to inhibit adipogenesis, providing complementary loss-of-function evidence for the role for TIMP3 in inhibiting adipogenesis. The finding that TIMP3 was required for the ability of Hh signaling to inhibit adipogenesis in 3T3-L1 cells indicates that TIMP3 operates downstream of or in parallel to Hh signaling.

How does TIMP3 inhibit adipogenesis? Although TIMP3 has MMP-independent functions (Nakajima et al., 2010; Qi et al., 2003), the ability of batimastat to mimic the effect of TIMP3 on adipogenesis suggests that it acts through MMPs to suppress intramuscular fat formation. Both TIMP3 and batimastat inhibit MMP14 (Hotary et al., 2002; Wei et al., 2005), and we found that inhibiting MMP14 function by either knockdown or pharmacological inhibitor blocked adipogenesis, consistent with previous data (Chun et al., 2006). Our finding that MMP14 functions downstream of or in parallel to TIMP3 suggests that TIMP3 represses adipogenesis through inhibition of MMP14. We propose that MMP14 selective inhibitors may provide a means of suppressing adipogenesis and improving muscle regeneration without incurring prohibitive adverse effects (Devy et al., 2009).

Following injury, MuSCs, supported by FAPs, produce new myofibers (Joe et al., 2010). In myopathies, such as DMD, chronic destruction leads to loss of large myofibers. Excitingly, loss of FAP cilia increases myofiber size, both after acute injury and in *DMD*^{mdx} mice, suggesting that FAP cilia influence myofiber regeneration. One mechanism by which FAP cilia may influence myogenesis is via the suppression of adipogenesis itself. Alternatively, ciliary Hh signaling may independently affect myogenesis, perhaps through TIMP3, a previously described modulator of myogenesis (Liu et al., 2010).

This work reveals that cilia have critical functions in coordinating adult skeletal muscle regeneration by interpreting Hh cues that direct FAP fate, that ciliary Hh signaling controls expression of the MMP inhibitor TIMP3, and that pharmacological modulation of MMP activity can inhibit intramuscular adipogenesis. Thus, our results reveal a mechanism by which cilia orchestrate intercellular communication during regeneration and point to new strategies to combat chronic muscle diseases.

STAR METHODS

CONTACT FOR REAGENT AND RESOURCE SHARING

Further information and requests for resources and reagents should be directed to and will be fulfilled by the Lead Contact, Jeremy Reiter (jeremy.reiter@ucsf.edu).

EXPERIMENTAL MODEL AND SUBJECT DETAILS

Animal Studies—*Ift88*^{tm1Bky}, *Gt*(*ROSA*)*26Sor*$^{tm1(EYFP)Cos}$ and *Ptch1*^{tm1Bjw} alleles have been described previously (Ellis et al., 2003; Haycraft et al., 2007; Srinivas et al., 2001). *Pdgfra*-CreERT mice (Tg(Pdgfrα-cre/ERT)467Dbe) were kindly provided by Dwight Bergles (Kang et al., 2010). *DMD*^{mdx} mice were purchased from the Jackson Laboratory (Stock No: 001801). Littermates lacking either the Cre, the null (in the case of *Ift88*) or the second floxed allele (in the case of *Ptch1*) served as controls, as these three controls displayed no differences in the number of intramuscular adipocytes in a range of experimental conditions (Figures S2B, S3A and S4C). Differences in intramuscular adipogenesis were observed in both male and female mice and, thus, both sexes were used included in experiments (Figure S2B). We have provided a list of all the genetically modified mice (gender and genotype) used per experiment (Table S2). For experiments using exclusively wild type mice, CD1 mice (Charles River) were used. Each mouse strain

was initially outcrossed 1–2 times to CD1 mice before intercrossing and maintained by breeding to CD1 mice. Thus, all mice used in this study are on a mixed genetic background. Tamoxifen (Sigma T-5648) was dissolved in corn oil and administered by oral gavage (200–250 mg/kg) on two consecutive days to 10–12 week old adults 2 weeks before injury. All DMD^{mdx} mice received 2 doses of tamoxifen at 4–5 weeks of age and were aged until 1 year of age. In addition, all control mice regardless of gender of genotype underwent the same tamoxifen treatment. For muscle injuries, mice were anesthetized with isoflurane and 25–50μl of 10 μM cardiotoxin (Sigma, C9759) or 50% glycerol was injected into the tibialis anterior muscle. For batimastat and SAG treatment in vivo, 10–12 week old CD1 mice were injected intraperitoneally with 2 mg/kg batimastat (Tocris) or 175 μg/kg SAG (EMD Millipore) on the day of injury and two days post injury (Heine et al., 2011; Macaulay et al., 1999). For proliferation studies, BrdU (50 μg/g body weight; Alfa Aesar) was administered either via intraperitoneal injection two hours before sacrificing or provided ad libitum via the drinking water (1 mg/ml) during the first 2 days post injury (Kopinke et al., 2012). All animal protocols were approved by the Institutional Animal Care and Use Committee (IACUC) of the University of California, San Francisco.

Cell Culture—3T3-L1 pre-adipocytes, a sub clone of NIH 3T3 cells, which were derived from a male Swiss albino mouse embryo, were purchased at passage 8 and cultured according to manufacturer's instructions (Zenbio). In brief, 3T3-L1 cells were cultured in preadipocyte medium comprised of high glucose Dulbecco's modified Eagle's medium (DMEM, Gibco), 10% newborn calf serum (Gibco) and GlutaMax (Gibco) and media was changed every other day. Two days after cells reached confluency, adipocyte differentiation medium comprised of DMEM, 10% fetal bovine serum (Gibco) and GlutaMax was added containing Insulin (0.862 μM; Sigma, I2643) and Troglitazone (5 μM; Sigma, T2573). After three days in differentiation medium, 3T3-L1 cells were switched to maintenance medium (DMEM, 10% FBS, GlutaMax and 0.862 μM Insulin) until analysis. SAG (3 or 100nM, EMD Millipore, #566660), batimastat (10 μM; Tocris), MMP2-inhibitor II (10 μM, Calbiochem), NSC405020 (100 μM, Sigma) or 0.1% DMSO (ATCC) were added at time of induction with Insulin and Troglitazone. Gene knockdown was achieved using the Silencer select pre-designed siRNAs according to the manufacturer's instructions (Thermofisher). Briefly, 3T3-L1 cells were transfected four days prior to adding the induction cocktail with either scRNA control (4390843, Thermofisher), siRNAs against *Timp3* (s75164 and s75165, Thermo Fisher Scientific), *Mmp14* (s69920), *Mmp16* (s69926) and *Mmp23* (s77255) using Lipofectamine RNAiMax (Thermo Fisher Scientific).

METHOD DETAILS

Histology, Immunohistochemistry and Image Analysis—Tissue fixation, processing and immunostaining were performed as described previously (Kopinke et al., 2011). In brief, tibialis anterior muscle was fixed in 4% paraformaldehyde (PFA) for 2 hrs at 4°C and cryopreserved with 30% sucrose overnight at 4C. One day later, muscles were embedded in OCT compound (Sakura Finetek) and snap frozen in liquid nitrogen-cooled isopentane. Muscles were cryosectioned at 10 μm at midbelly and 3–4 sections collected every 250–350 μm. The most representative of all sections was used for quantifying the number of adipocytes, while randomly selected images across all sections were recorded for

all other quantifications. 3T3-L1s or MACS-purified FAPs, grown on glass cover slips, were fixed in 4% PFA for 10min. Sections and cells were incubated with primary antibodies in blocking solution (5% donkey serum in PBS with 0.3% Triton X-100) overnight at 4°C. To visualize BrdU, slides were treated with 800 U/ml DNase I for 20 min at room temperature in 40 mM Tris HCL (pH 7.4), 10 mM NaCl, 6 mM $MgCl_2$ and 10 mM $CaCl_2$ as previously described (Kopinke et al., 2012). To visualize γ-TUBULIN, tissue sections were incubated with 1% SDS in PBS for 5 min. Antigen retrieval using a Sodium Citrate Buffer (10mM Sodium Citrate, 0.05% Tween 20, pH 6.0) was required for PAX7 and MYH3. Primary antibodies used were: rabbit anti-ARL13b (1:1000, Proteintech #17711-1-AP), Rabbit anti-LAMININ (1:1000, Sigma #L9393), rabbit anti-NINEIN (1:10000, gift from James Sillibourne), goat anti-PDGFRα (1:250, R&D Systems #AF1062), chicken anti-GFP (1:1000, Avis lab #1020), rabbit anti-PERILIPIN (1:1000, Cell Signaling #9349), rabbit anti-FABP4 (1:500, Proteintech # 51035-1-AP), rabbit anti-DHH (1:1000, Genetex #GTX109762), rat anti-BrdU (1:1000, Abcam #AB6326), rabbit anti-cleaved CASPASE3 (1:250, Cell Signaling # 9664), mouse anti-TUB^{Ac} (1:1000, Sigma #T6793), mouse anti-PAX7 (1:100, Developmental Studies Hybridoma Bank), mouse anti-MYH3 (1:100, Developmental Studies Hybridoma Bank # F1.652) and goat anti-γTUBULIN (1:250, Santa Cruz #SC-7396). Alexa Fluor-conjugated secondary antibodies from Life Technologies (1:1000) in combination with directly conjugated probes Phalloidin-Alexa 647 (1:100, Molecular Probes # A22287) and wheat germ agglutinin (WGA)-Alexa 647 (Molecular Probes, #W32466) were added for 2 hrs at room temperature. DAPI (Sigma) was used to visualize nuclei. Oil Red O staining was performed according to manufacturer's instructions (Lonza). Images from randomly chosen fields across several sections (each 250–350 μm apart) were acquired using a Leica SPE confocal microscope or a Zeiss Observer D1 microscope with an Axiocam MRc camera. The tiling function within the Leica LSA software was used to generate the cross-sectional images of whole tibialis anterior muscles. All images were processed identically with Adobe Photoshop (CS5). ImageJ (v1.50b) was used to quantify the area occupied by Oil Red O positive adipocytes. In brief, images were converted to binary images using the Threshold function, followed by using watershed and area occupied quantified using the Analyze Particle function (size at 0.0005-inf and circularity at 0.2–1). DMSO or scRNA controls were set to 100% with the experimental samples normalized to the controls. For cross sectional area measurements of fibers, LAMININ and Phalloidin stained muscle sections were thresholded and fiber areas quantified using analyze particle function in ImageJ. For color coding of fibers based on size, the ROI Color Coder function was used (http://imagejdocu.tudor.lu/doku.php?id=macro:roi_color_coder). To quantify cilia, images with a Z resolution between 2–3 nm were randomly taken and primary cilia were identified by either the axonemal component acetylated tubulin (TUB^{AC}) or the ciliary membrane marker ARL13B, while basal bodies were identified by NINEIN or γ-TUBULIN. To measure adipocyte size, we determined the diameter of adipocytes, as marked by FABP4, in 3–4 randomly taken 40x images from 3 control and 3 $FAP^{no\ cilia}$ mice.

Expression Studies—Whole muscle tissue was placed in in TRIzol (Thermofisher) and disrupted using the TissueLyser II (Qiagen). Cells were placed in buffer RLT and vortexed and RNA was isolated using the Qiagen RNeasy kit. 100–250ng RNA was used to make

cDNA (iScript cDNA synthesis kit, Bio-Rad). RT-qPCR was performed in technical triplicates on an ABI 7900HT real-time PCR machine (Applied Biosystems) using the EXPRESS SYBR GreenER 2X master mix (Invitrogen). Fold changes were calculated using the $2^{-\Delta\Delta ct}$ method (Schmittgen and Livak, 2008) and expression levels normalized to the average of the housekeeping genes *Hprt*, *Dolk*, *Pde12* and *Sra1*. Primer sequences used in this study are listed in Table S3. For RNAseq, a total of 5 control and 3 $FAP^{no\ cilia}$ samples were used. For each sample, tibialis anterior muscles from 2–4 mice were combined and FAPs were MACS-purified. To maximize yield, TA's on both sides were injured and used. The TruSeq Stranded Total RNA Library Prep Kit (Ilumina) was used to generate the library, which was subsequently sequenced using an Illumina 2500 SE 50bp platform and aligned to the GRCm38.78 whole genome using STAR RNAseq aligner. Individual read counts were normalized to the geometric mean read count across all samples using DEseq. Using a cutoff of $p<0.05$ and neglecting genes with less than 100 reads, 609 genes were identified. To enrich for likely Hh targets, these 609 genes were cross-referenced against five known Hh target lists (Table S1) (Falkenstein and Vokes, 2014; Hsu et al., 2014; Ingram et al., 2002; Valin et al., 2009; Yu et al., 2009).

Cell Lysis and Immunoblot—MACS-isolated FAPs from tibialis anterior muscle were lysed at 4°C using RIPA buffer (50mM Tris-HCl pH 7.4, 150mM NaCl, 0.1% SDS, 0.5% sodium deoxycholate, 1% NP-40, protease and phosphatase inhibitors (Calbiochem and Roche, respectively). Cell lysates were cleared by centrifugation at 16,000 *g* for 10 min, and protein concentration was determined using a BCA assay (Thermo Fisher Scientific). The cell lysate was denatured at 100°C for 5 min in 6X SDS-PAGE loading buffer. 5–10 μg of cell lysates were resolved on 4–15% TGX gradient gels (Bio-Rad Laboratories) and transferred to nitrocellulose membrane (Amersham). Membranes were blocked with 5% non-fat dried milk in TBS with 0.1% Tween, and then incubated with primary antibody overnight at 4°C. Primary antibodies used were mouse anti-GLI3 (1:1,000; gift of Suzie Scales, Genentech) and mouse anti-αTUB (1:5000; Sigma #T5168). After washing in TBS with 0.1% Tween, membranes were incubated in HRP-conjugated secondary antibody for 2hr at room temperature. Blots were developed with Western lightning enhanced chemiluminescence (PerkinElmer), and molecular weights were determined using full-range rainbow pre-stained protein standards (GE Healthcare).

Magnetic activated cell sorting—Magnetic activated cell sorting (MACS) of FAPs was performed as previously described (Heredia et al., 2013). Briefly, tibialis anterior muscle were finely minced on ice with a scalpel and digested in Ham's F10 medium containing 0.016% Collagenase II (Gibco) for 45 min in a shaking 37°C air incubator. The cell suspension was filtered through a 100 and 40 μM filter and red blood cells were removed. For negative selection, suspended cells were incubated with biotinylated antibodies (~0.5 μg/μL) against anti-Integrin α7, anti-CD3 and anti-CD45 (Biolegend), followed by incubation with anti-Biotin microbeads. Samples were then run through LD columns (Miltenyi Biotec) followed by two washes with MACS buffer (0.5 % BSA and 2.5 mM EDTA in dPBS). Unlabeled cells were collected and incubated with an anti-Sca1-PE antibody (Biolegend) followed by anti-PE microbeads (Miltenyi Biotec). Sca1-labeled cells

were collected using LS columns (Miltenyi Biotec). After three washes with MACS buffer, cells were eluted and used for downstream applications.

QUANTIFICATION AND STATISTICAL ANALYSIS

3–6 biological replicates were used for all cell culture experiments and all experiments were repeated at least twice. All data were analyzed with GraphPad Prism (version 7) and represented as mean ± SEM. A paired two-tailed t test was used for two samples with a single variable. For more than two samples, one-way ANOVA followed by a Dunnett's multiple comparison test for one variable or a two-way ANOVA followed by Tukey's multiple comparison test for two variables was used. A p value less than 0.05 was considered statistically significant and are denoted as follows: *<0.05, **<0.01, ***<0.001 and ****<0.0001.

DATA AND SOFTWARE AVAILABILITY

The raw data of the RNAseq experiment have been deposited to NCBI Geo (GSE86073).

Supplementary Material

Refer to Web version on PubMed Central for supplementary material.

Acknowledgments

We thank E Yu for assistance with mouse husbandry, and members of the Reiter laboratory for critical discussion, Nadja Makki, Brian Black and Andrew Brack for helpful comments on the manuscript, Elaine Carlson for providing help with expression studies and mouse genotyping, and Ajay Chawla and members of his laboratory for assistance with MACS. We acknowledge the UCSF Functional Genomics Core Facility for assistance with RNAseq. This work was supported by grants from the NIH (AR054396 and GM095941), the Burroughs Wellcome Fund and the Packard Foundation to J.F.R. E.C.R. was supported by the ARCS Foundation, Northern California Chapter. D.K. was supported by a Development Grant from the Muscular Dystrophy Association.

References

Bauters D, Scroyen I, Van Hul M, Lijnen HR. Gelatinase A (MMP-2) promotes murine adipogenesis. Biochim Biophys Acta. 2015; 1850:1449–1456. [PubMed: 25869489]

Bernot D, Barruet E, Poggi M, Bonardo B, Alessi MC, Peiretti F. Down-regulation of tissue inhibitor of metalloproteinase-3 (TIMP-3) expression is necessary for adipocyte differentiation. J Biol Chem. 2010; 285:6508–6514. [PubMed: 20056610]

Brownell I, Guevara E, Bai CB, Loomis CA, Joyner AL. Nerve-derived sonic hedgehog defines a niche for hair follicle stem cells capable of becoming epidermal stem cells. Cell Stem Cell. 2011; 8:552–565. [PubMed: 21549329]

Bulfield G, Siller WG, Wight PA, Moore KJ. X chromosome-linked muscular dystrophy (mdx) in the mouse. Proc Natl Acad Sci U S A. 1984; 81:1189–1192. [PubMed: 6583703]

Chavey C, Mari B, Monthouel MN, Bonnafous S, Anglard P, Van Obberghen E, Tartare-Deckert S. Matrix metalloproteinases are differentially expressed in adipose tissue during obesity and modulate adipocyte differentiation. J Biol Chem. 2003; 278:11888–11896. [PubMed: 12529376]

Chen JK, Taipale J, Young KE, Maiti T, Beachy PA. Small molecule modulation of Smoothened activity. Proc Natl Acad Sci U S A. 2002; 99:14071–14076. [PubMed: 12391318]

Chun TH, Hotary KB, Sabeh F, Saltiel AR, Allen ED, Weiss SJ. A pericellular collagenase directs the 3-dimensional development of white adipose tissue. Cell. 2006; 125:577–591. [PubMed: 16678100]

d'Albis A, Couteaux R, Janmot C, Roulet A, Mira JC. Regeneration after cardiotoxin injury of innervated and denervated slow and fast muscles of mammals. Myosin isoform analysis. Eur J Biochem. 1988; 174:103–110. [PubMed: 3371354]

Devy L, Huang L, Naa L, Yanamandra N, Pieters H, Frans N, Chang E, Tao Q, Vanhove M, Lejeune A, et al. Selective inhibition of matrix metalloproteinase-14 blocks tumor growth, invasion, and angiogenesis. Cancer Res. 2009; 69:1517–1526. [PubMed: 19208838]

Dulor JP, Cambon B, Vigneron P, Reyne Y, Nougues J, Casteilla L, Bacou F. Expression of specific white adipose tissue genes in denervation-induced skeletal muscle fatty degeneration. FEBS Letters. 1998; 439:89–92. [PubMed: 9849884]

Ellis T, Smyth I, Riley E, Graham S, Elliot K, Narang M, Kay GF, Wicking C, Wainwright B. Patched 1 conditional null allele in mice. Genesis. 2003; 36:158–161. [PubMed: 12872247]

Falkenstein KN, Vokes SA. Transcriptional regulation of graded Hedgehog signaling. Semin Cell Dev Biol. 2014; 33:73–80. [PubMed: 24862856]

Goetz SC, Anderson KV. The primary cilium: a signalling centre during vertebrate development. Nat Rev Genet. 2010; 11:331–344. [PubMed: 20395968]

Goodrich LV, Milenkovic L, Higgins KM, Scott MP. Altered neural cell fates and medulloblastoma in mouse patched mutants. Science. 1997; 277:1109–1113. [PubMed: 9262482]

Haycraft CJ, Zhang Q, Song B, Jackson WS, Detloff PJ, Serra R, Yoder BK. Intraflagellar transport is essential for endochondral bone formation. Development. 2007; 134:307–316. [PubMed: 17166921]

Heine VM, Griveau A, Chapin C, Ballard PL, Chen JK, Rowitch DH. A small-molecule smoothened agonist prevents glucocorticoid-induced neonatal cerebellar injury. Sci Transl Med. 2011; 3:105ral04.

Heredia JE, Mukundan L, Chen FM, Mueller AA, Deo RC, Locksley RM, Rando TA, Chawla A. Type 2 innate signals stimulate fibro/adipogenic progenitors to facilitate muscle regeneration. Cell. 2013; 153:376–388. [PubMed: 23582327]

Hoffman EP, Brown RH, Kunkel LM. Dystrophin - the Protein Product of the Duchenne Muscular-Dystrophy Locus. Cell. 1987; 51:919–928. [PubMed: 3319190]

Hotary KB, Yana I, Sabeh F, Li XY, Holmbeck K, Birkedal-Hansen H, Allen ED, Hiraoka N, Weiss SJ. Matrix metalloproteinases (MMPs) regulate fibrin-invasive activity via MT1-MMP-dependent and -independent processes. J Exp Med. 2002; 195:295–308. [PubMed: 11828004]

Hsu YC, Li L, Fuchs E. Transit-amplifying cells orchestrate stem cell activity and tissue regeneration. Cell. 2014; 157:935–949. [PubMed: 24813615]

Hu JK, McGlinn E, Harfe BD, Kardon G, Tabin CJ. Autonomous and nonautonomous roles of Hedgehog signaling in regulating limb muscle formation. Genes Dev. 2012; 26:2088–2102. [PubMed: 22987639]

Hui CC, Angers S. Gli proteins in development and disease. Annu Rev Cell Dev Biol. 2011; 27:513–537. [PubMed: 21801010]

Ingram WJ, Wicking CA, Grimmond SM, Forrest AR, Wainwright BJ. Novel genes regulated by Sonic Hedgehog in pluripotent mesenchymal cells. Oncogene. 2002; 21:8196–8205. [PubMed: 12444557]

Joe AW, Yi L, Natarajan A, Le Grand F, So L, Wang J, Rudnicki MA, Rossi FM. Muscle injury activates resident fibro/adipogenic progenitors that facilitate myogenesis. Nat Cell Biol. 2010; 12:153–163. [PubMed: 20081841]

Kang SH, Fukaya M, Yang JK, Rothstein JD, Bergles DE. NG2+ CNS glial progenitors remain committed to the oligodendrocyte lineage in postnatal life and following neurodegeneration. Neuron. 2010; 68:668–681. [PubMed: 21092857]

Khokha R, Murthy A, Weiss A. Metalloproteinases and their natural inhibitors in inflammation and immunity. Nat Rev Immunol. 2013; 13:649–665. [PubMed: 23969736]

Kopinke D, Brailsford M, Pan FC, Magnuson MA, Wright CV, Murtaugh LC. Ongoing Notch signaling maintains phenotypic fidelity in the adult exocrine pancreas. Dev Biol. 2012; 362:57–64. [PubMed: 22146645]

Kopinke D, Brailsford M, Shea JE, Leavitt R, Scaife CL, Murtaugh LC. Lineage tracing reveals the dynamic contribution of Hesl$_+$ cells to the developing and adult pancreas. Development. 2011; 138:431–441. [PubMed: 21205788]

Kramann R, Schneider RK, DiRocco DP, Machado F, Fleig S, Bondzie PA, Henderson JM, Ebert BL, Humphreys BD. Perivascular GH1+ progenitors are key contributors to injury-induced organ fibrosis. Cell Stem Cell. 2015; 16:51–66. [PubMed: 25465115]

Lemos DR, Babaeijandaghi F, Low M, Chang CK, Lee ST, Fiore D, Zhang RH, Natarajan A, Nedospasov SA, Rossi FM. Nilotinib reduces muscle fibrosis in chronic muscle injury by promoting TNF-mediated apoptosis of fibro/adipogenic progenitors. Nat Med. 2015; 21:786–794. [PubMed: 26053624]

Liu A, Wang B, Niswander LA. Mouse intraflagellar transport proteins regulate both the activator and repressor functions of Gli transcription factors. Development. 2005; 132:3103–3111. [PubMed: 15930098]

Liu H, Chen SE, Jin B, Carson JA, Niu A, Durham W, Lai JY, Li YP. TIMP3: a physiological regulator of adult myogenesis. J Cell Sci. 2010; 123:2914–2921. [PubMed: 20682640]

Macaulay VM, O'Byrne KJ, Saunders MP, Braybrooke JP, Long L, Gleeson F, Mason CS, Harris AL, Brown P, Talbot DC. Phase I study of intrapleural batimastat (BB-94), a matrix metalloproteinase inhibitor, in the treatment of malignant pleural effusions. Clin Cancer Res. 1999; 5:513–520. [PubMed: 10100701]

Mariman EC, Wang P. Adipocyte extracellular matrix composition, dynamics and role in obesity. Cell Mol Life Sci. 2010; 67:1277–1292. [PubMed: 20107860]

Marion V, Stoetzel C, Schlicht D, Messaddeq N, Koch M, Flori E, Danse JM, Mandel JL, Dollfus H. Transient ciliogenesis involving Bardet-Biedl syndrome proteins is a fundamental characteristic of adipogenic differentiation. Proc Natl Acad Sci U S A. 2009; 106:1820–1825. [PubMed: 19190184]

May SR, Ashique AM, Karlen M, Wang B, Shen Y, Zarbalis K, Reiter J, Ericson J, Peterson AS. Loss of the retrograde motor for I FT disrupts localization of Smo to cilia and prevents the expression of both activator and repressor functions of Gli. Dev Biol. 2005; 287:378–389. [PubMed: 16229832]

McDonald AA, Hebert SL, Kunz MD, Ralles SJ, McLoon LK. Disease course in mdx:utrophin+/−mice: comparison of three mouse models of Duchenne muscular dystrophy. Physiol Rep. 2015:3.

Mitchell WK, Williams J, Atherton P, Larvin M, Lund J, Narici M. Sarcopenia, dynapenia, and the impact of advancing age on human skeletal muscle size and strength; a quantitative review. Front Physiol. 2012; 3:260. [PubMed: 22934016]

Montani JP, Carroll JF, Dwyer TM, Antic V, Yang Z, Dulloo AG. Ectopic fat storage in heart, blood vessels and kidneys in the pathogenesis of cardiovascular diseases. Int J Obes Relat Metab Disord. 2004; 28(Suppl 4):S58–65. [PubMed: 15592488]

Nakajima H, Ito M, Smookler DS, Shibata F, Fukuchi Y, Morikawa Y, Ikeda Y, Arai F, Suda T, Khokha R, et al. TIMP-3 recruits quiescent hematopoietic stem cells into active cell cycle and expands multipotent progenitor pool. Blood. 2010; 116:4474–4482. [PubMed: 20798233]

Piccioni A, Gaetani E, Neri V, Gatto I, Palladino M, Silver M, Smith RC, Giarretta I, Pola E, Hlatky L, et al. Sonic hedgehog therapy in a mouse model of age-associated impairment of skeletal muscle regeneration. J Gerontol A Biol Sci Med Sci. 2014a; 69:245–252. [PubMed: 23781099]

Piccioni A, Gaetani E, Palladino M, Gatto I, Smith RC, Neri V, Marcantoni M, Giarretta I, Silver M, Straino S, et al. Sonic hedgehog gene therapy increases the ability of the dystrophic skeletal muscle to regenerate after injury. Gene Ther. 2014b; 21:413–421. [PubMed: 24572787]

Pinnick KE, Collins SC, Londos C, Gauguier D, Clark A, Fielding BA. Pancreatic ectopic fat is characterized by adipocyte infiltration and altered lipid composition. Obesity (Silver Spring). 2008; 16:522–530. [PubMed: 18239594]

Pisani DF, Bottema CD, Butori C, Dani C, Dechesne CA. Mouse model of skeletal muscle adiposity: a glycerol treatment approach. Biochem Biophys Res Commun. 2010; 396:767–773. [PubMed: 20457129]

Pospisilik JA, Schramek D, Schnidar H, Cronin SJ, Nehme NT, Zhang X, Knauf C, Cani PD, Aumayr K, Todoric L, et al. Drosophila genome-wide obesity screen reveals hedgehog as a determinant of brown versus white adipose cell fate. Cell. 2010; 140:148–160. [PubMed: 20074523]

Przybylski RJ. Occurrence of Centrioles during Skeletal and Cardiac Myogenesis. The Journal of Cell Biology. 1971; 49:214–221. [PubMed: 5555575]

Qi JH, Ebrahem Q, Moore N, Murphy G, Claesson-Welsh L, Bond M, Baker A, Anand-Apte B. A novel function for tissue inhibitor of metalloproteinases-3 (TIMP3): inhibition of angiogenesis by blockage of VEGF binding to VEGF receptor-2. Nat Med. 2003; 9:407–415. [PubMed: 12652295]

Renault MA, Chapouly C, Yao Q, Larrieu-Lahargue F, Vandierdonck S, Reynaud A, Petit M, Jaspard-Vinassa B, Belloc I, Traiffort E, et al. Desert hedgehog promotes ischemia-induced angiogenesis by ensuring peripheral nerve survival. Circ Res. 2013; 112:762–770. [PubMed: 23343527]

Schmittgen TD, Livak KJ. Analyzing real-time PCR data by the comparative CT method. Nature Protocols. 2008; 3:1101–1108. [PubMed: 18546601]

Serrano AL, Mann CJ, Vidal B, Ardite E, Perdiguero E, Munoz-Canoves P. Cellular and molecular mechanisms regulating fibrosis in skeletal muscle repair and disease. Curr Top Dev Biol. 2011; 96:167–201. [PubMed: 21621071]

Srinivas S, Watanabe T, Lin CS, William CM, Tanabe Y, Jessell TM, Costantini F. Cre reporter strains produced by targeted insertion of EYFP and ECFP into the ROSA26 locus. BMC Dev Biol. 2001; 1:4. [PubMed: 11299042]

Straface G, Aprahamian T, Flex A, Gaetani E, Biscetti F, Smith RC, Pecorini G, Pola E, Angelini F, Stigliano E, et al. Sonic hedgehog regulates angiogenesis and myogenesis during post-natal skeletal muscle regeneration. J Cell Mol Med. 2009; 13:2424–2435. [PubMed: 18662193]

Suh JM, Gao X, McKay J, McKay R, Salo Z, Graff JM. Hedgehog signaling plays a conserved role in inhibiting fat formation. Cell Metab. 2006; 3:25–34. [PubMed: 16399502]

Uezumi A, Fukada S, Yamamoto N, Takeda S, Tsuchida K. Mesenchymal progenitors distinct from satellite cells contribute to ectopic fat cell formation in skeletal muscle. Nat Cell Biol. 2010; 12:143–152. [PubMed: 20081842]

Uezumi A, Ito T, Morikawa D, Shimizu N, Yoneda T, Segawa M, Yamaguchi M, Ogawa R, Matev MM, Miyagoe-Suzuki Y, et al. Fibrosis and adipogenesis originate from a common mesenchymal progenitor in skeletal muscle. J Cell Sa. 2011; 124:3654–3664.

Valin A, Barnay-Verdier S, Robert T, Ripoche H, Brellier F, Chevallier-Lagente O, Avril MF, Magnaldo T. PTCH1 +/− dermal fibroblasts isolated from healthy skin of Gorlin syndrome patients exhibit features of carcinoma associated fibroblasts. PLoS One. 2009; 4:e4818. [PubMed: 19287498]

Wei S, Kashiwagi M, Kota S, Xie Z, Nagase H, Brew K. Reactive site mutations in tissue inhibitor of metalloproteinase-3 disrupt inhibition of matrix metalloproteinases but not tumor necrosis factor-alpha-converting enzyme. J Biol Chem. 2005; 280:32877–32882. [PubMed: 16079149]

Yu M, Gipp J, Yoon JW, lannaccone P, Walterhouse D, Bushman W. Sonic hedgehog-responsive genes in the fetal prostate. J Biol Chem. 2009; 284:5620–5629. [PubMed: 19095649]

Zhu D, Shi S, Wang H, Liao K. Growth arrest induces primary-cilium formation and sensitizes IGF-1-receptor signaling during differentiation induction of 3T3-L1 preadipocytes. J Cell Sci. 2009; 122:2760–2768. [PubMed: 19596798]

HIGHLIGHTS

- Fibro/adipogenic progenitors (FAPs) are dynamically ciliated during regeneration
- Ciliary Hh signaling restricts FAP conversion into adipocytes through TIMP3
- TIMP3 represses injury-induced adipogenesis through inhibition of MMP14
- Removal of cilia from FAPs enhances myofiber size and formation following injury

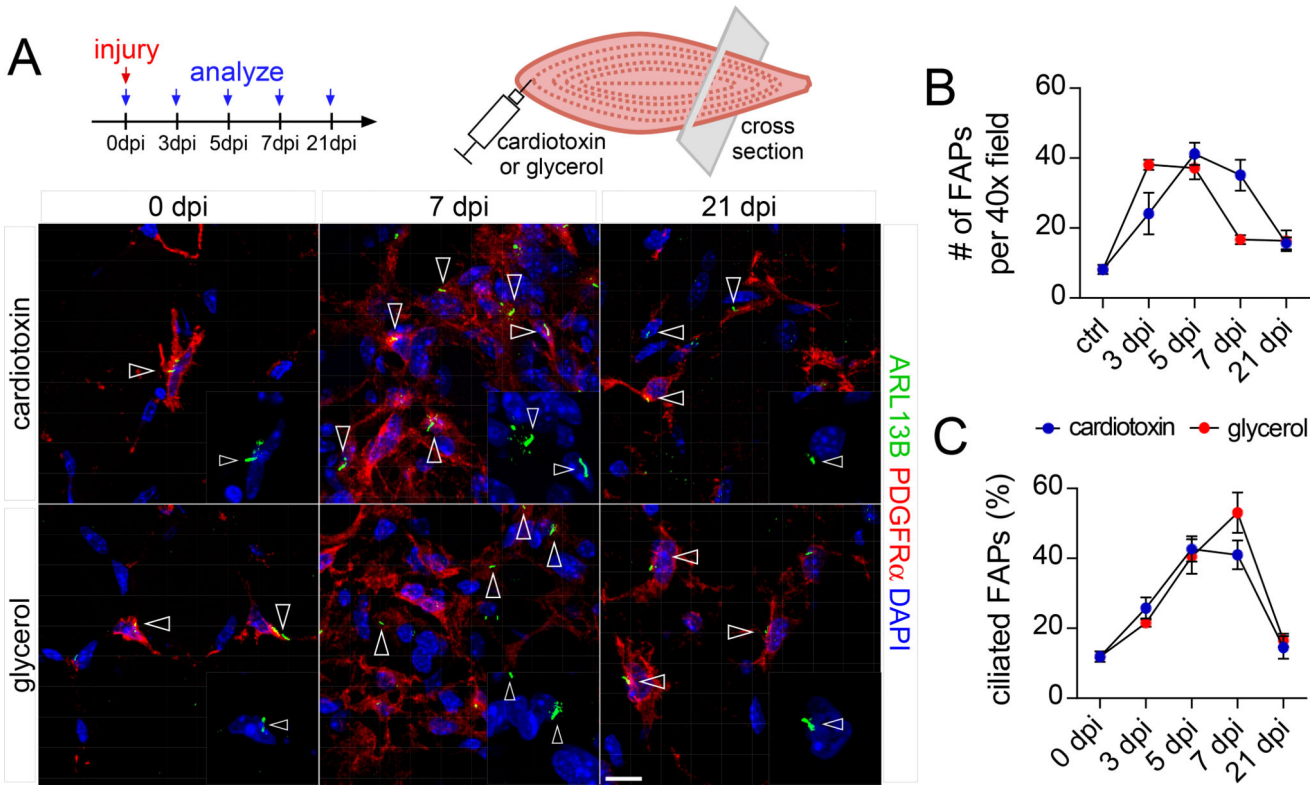

Figure 1. FAPs are dynamically ciliated during muscle regeneration

(A) Immunofluorescence for cilia (ARL13B, green) and FAPs (PDGFRα, red) at the indicated time points after injury with cardiotoxin (top row) or glycerol (bottom row) of the tibialis anterior muscle of wild type mice (n=3–7 mice per time point and per injury). Ciliated FAPs are marked by arrowheads. Nuclei are stained with DAPI (blue). Scale bar is 10 μm.

(B) Quantifications of the total number of FAPs present per 40x view at the indicated time points after injury (n=3–7 mice per time point and per injury).

(C) Quantifications of the percentage of ciliated FAPs over total FAPs (n=3–7 mice per time point and per injury). All data are represented as mean ± SEM. See also Figure S1.

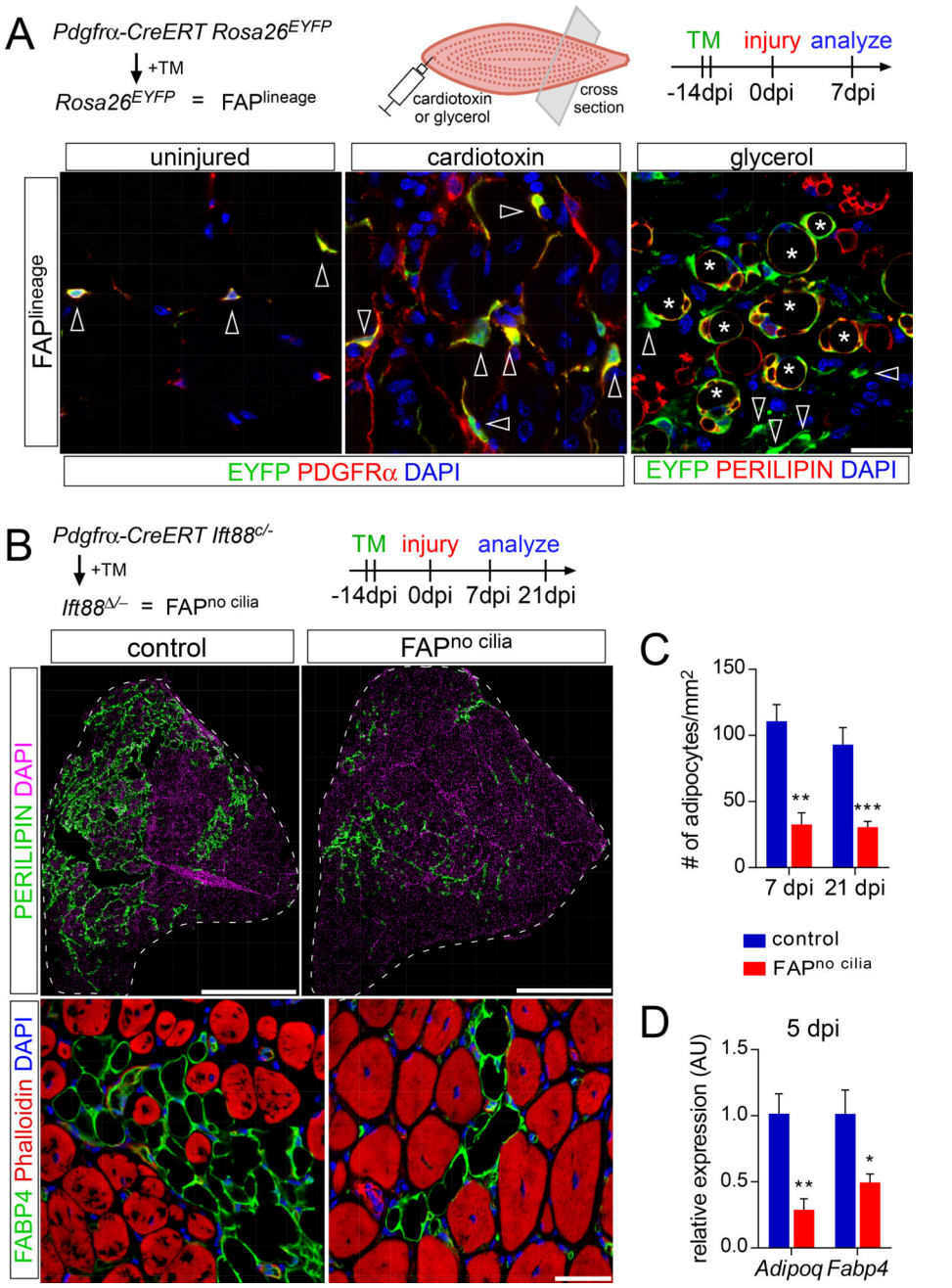

Figure 2. Removing FAP cilia impairs fat formation

(A) Detection of lineage label (EYFP, green) in FAPs (arrowheads; PDGFRα, red) 7 dpi with cardiotoxin injection and in adipocytes (asterisks; PERILIPIN, red) 7 dpi with glycerol injection using *PDGFRα*-CreERT *Rosa26*^{EYFP} mice. Scale bar is 25 μm.

(B) Immunofluorescence for adipocytes (PERILIPIN, top, green or FABP4, bottom, red) 21 dpi with glycerol injection after conditional removal of FAP cilia (n=8–12 mice per genotype). Nuclei are stained with DAPI. Myofibers are stained with phalloidin (red). Scale bars are 1 mm (top) and 25 μm (bottom).

(C) Quantifications of the number of adipocytes present per 1 mm^2 of injured area 7 dpi (n=4 per genotype) or 21 dpi with glycerol injection (n=8–12 per genotype).
(D) RT-qPCR for mature adipocyte markers (*Adipoq* and *Fabp4*) from whole muscle RNA 5 dpi with glycerol injection (n=4 per genotype). All data are represented as mean ± SEM. See also Figure S2.

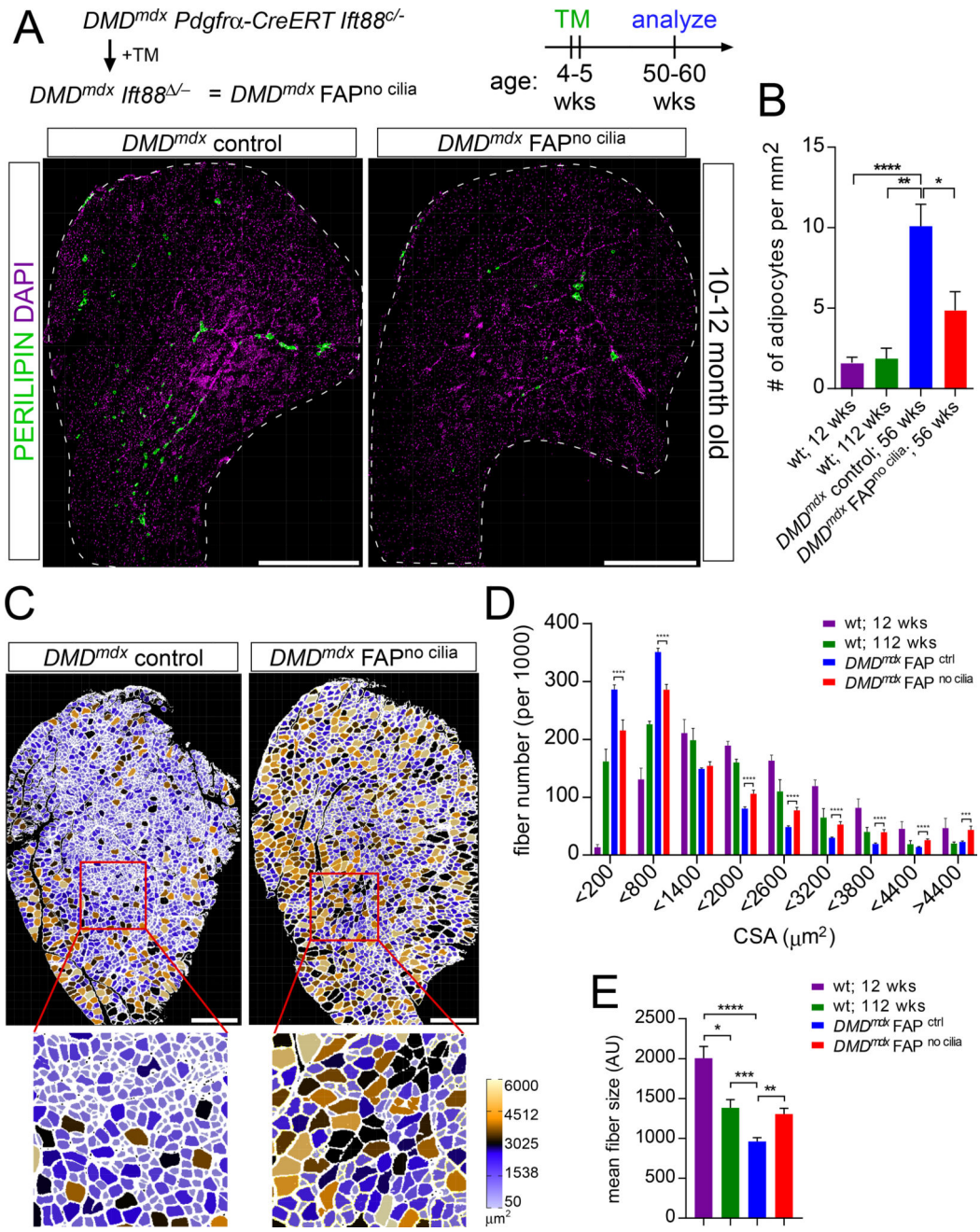

Figure 3. Loss of FAP cilia reduces fatty degeneration of *Dmd*^{mdx} muscle

(A) Immunofluorescence for adipocytes (PERILIPIN, green) after conditional removal of FAP cilia in 10–12 month old *DMD*^{mdx} mice. Scale bar is 1 mm.

(B) Quantifications of the number of adipocyte present per 1 mm^2 of tibialis anterior muscle in 12 week old wild type mice (n=10), 2 year old wild type mice (n=5), 1 year old *DMD*^{mdx} control mice (n=17) and *DMD*^{mdx} FAP$^{no\ cilia}$ mice (n=8).

(C) Myofibers of 10–12 month old *DMD*^{mdx} FAP$^{no\ cilia}$ and *DMD*^{mdx} control mice color-coded based on size of cross-sectional area using the ROI Color Coder function in ImageJ (see Experimental Procedures for details). Scale bar is 0.5 mm.

(D) Distribution of the number of fibers based on their cross-sectional area in 12 week old (n=7) and 2 year old (n=5) wild type and *DMD*^{mdx} mice with cilia (n=11) and no cilia (n=5). (E) Average cross-sectional area size of myofibers from wild type (n=7 for 12 week old and n=5 for 2 year old), *DMD*^{mdx} FAP$^{\text{no cilia}}$ (n=5) and *DMD*^{mdx} control mice (n=11). All data are represented as mean ± SEM. See also Figure S3.

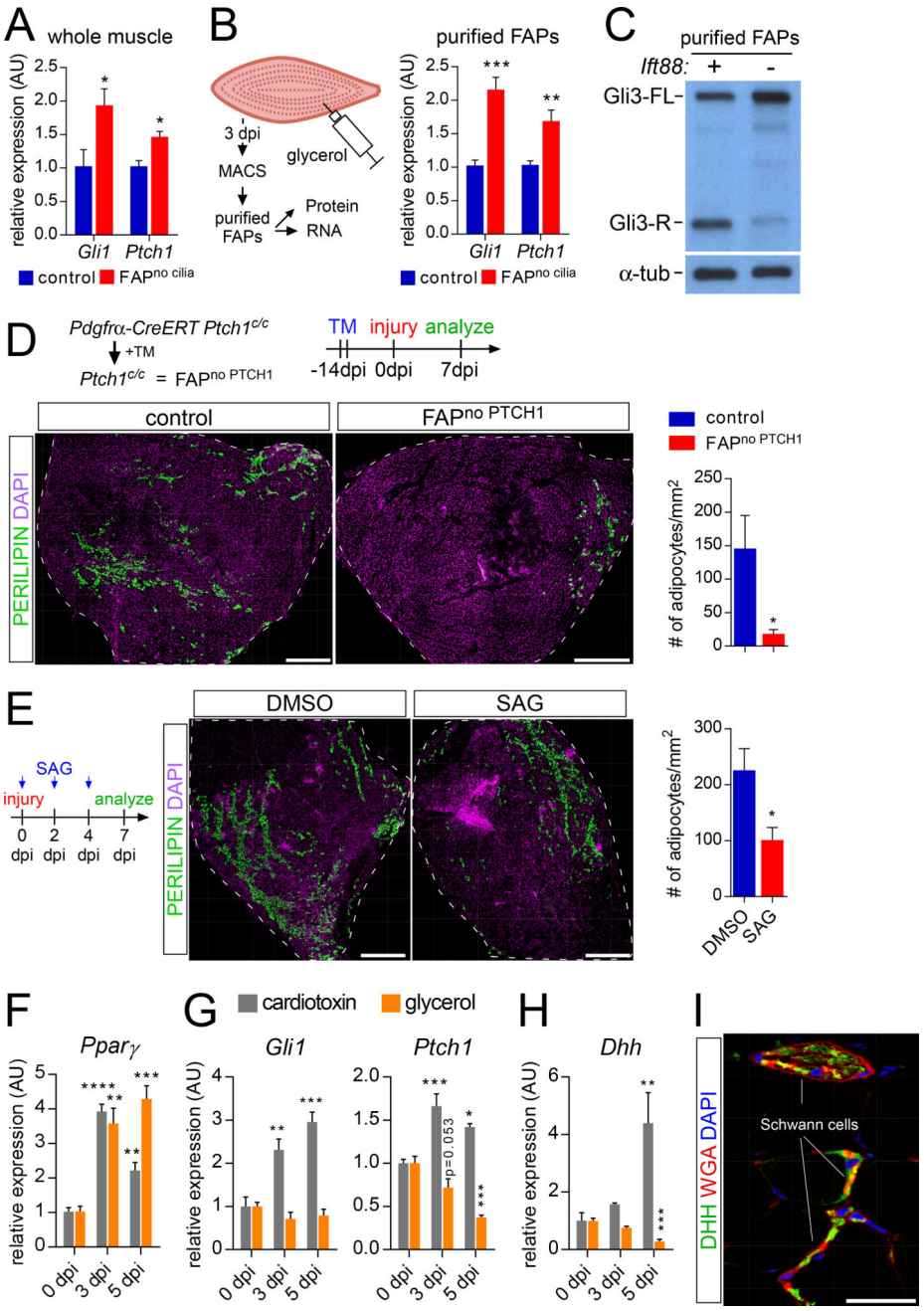

Figure 4. FAP cilia repress Hh target genes

(A) *Gli1* and *Ptch1* RT-qPCR from whole muscle of control (n=4) and FAP$^{no\ cilia}$ mice (n=4) 5 dpi with glycerol injection.

(B) *Gli1* and *Ptch1* RT-qPCR from MACS-purified FAPS of control (n=5) and FAP$^{no\ cilia}$ mice (n=6) 3 dpi with glycerol injection.

(C) Immunoblotting for GLI3 and α-TUBULIN (loading control) on whole cell protein lysates from MACS-purified FAPs of control and FAP$^{no\ cilia}$ mice at 3 dpi with glycerol injection (n=10–12 per genotype per sample).

(D) Immunofluorescence for adipocytes (PERILIPIN, green) after conditional removal of *Ptch1* in FAPs 7 dpi with glycerol injection. Scale bar is 500 μm. Right: Quantifications of the number of adipocyte present per 1 mm^2 of injured muscle from control (n=7) and $FAP^{no\ PTCH1}$ (n=7) mice 7 dpi.

(E) Immunofluorescence of adipocytes (PERILIPIN, green) of wild type mice tibialis anterior muscle 7 dpi with injection of glycerol and either DMSO or SAG at day 0, 2 and day 4. Scale bar is 500 μm. Right: Quantifications of number of adipocytes per mm^2 of injured area 7 dpi (n= 5–9 per treatment group).

(F–I) RT-qPCR analysis of RNA isolated from whole tibialis anterior muscle without injury or 3 and 5 dpi with injection of cardiotoxin (gray) or glycerol (orange) (n=4 per time point and injury) for (F) *Pparγ*, (G) *Gli1* and *Ptch1* and (H) *Dhh*.

(I) Immunofluorescence for DHH (green) and Schwann cells (WGA, red) in uninjured tibialis anterior muscle. Scale bar is 50 μm. All data are represented as mean ± SEM. See also Figure S4.

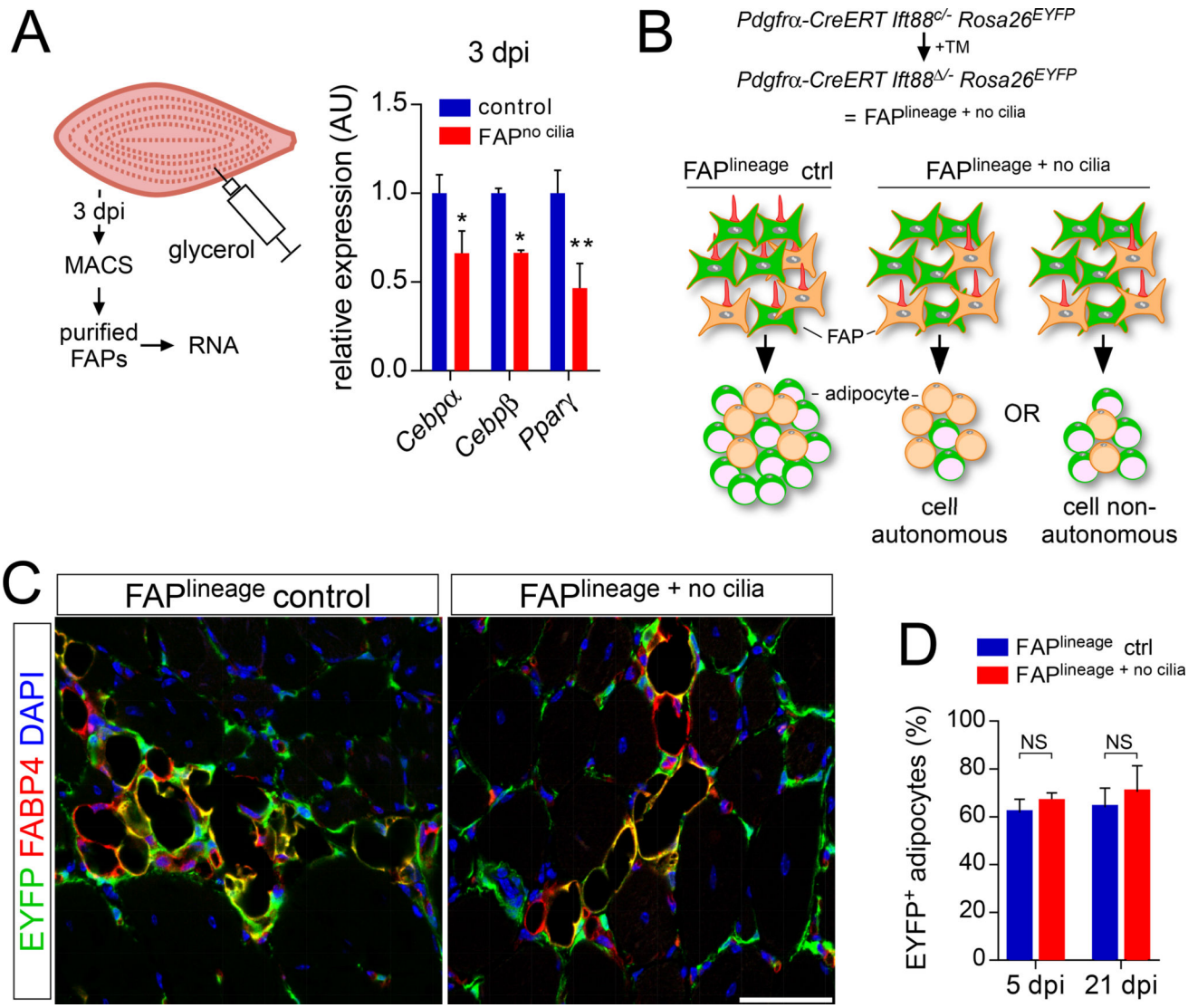

Figure 5. Ciliary Hh signaling reduces adipocyte differentiation via a cell non-autonomous mechanism

(A) RT-qPCR analysis of MACS-purified FAPs of control and FAP$^{\text{no cilia}}$ mice 3 dpi with glycerol injection (n=5–6 per genotype) for the early adipocyte genes *Cebpa, Cebpβ* and *Pparγ*.

(B) Combining the *Rosa26*^{EYFP} allele with *Pdgfra*-CreERT *Ift88*$^{c/-}$ mice allows for simultaneous deletion of cilia and activation of the lineage mark. A specific reduction in the percentage of EYFP^{+} adipocytes (green) would argue for a cell autonomous effect after loss of FAP cilia, whereas a reduction in total number of both EYFP^{+} and EYFP^{-} adipocytes (without affecting the percentage expressing EYFP) would suggest a cell non-autonomous mechanism.

(C) Immunofluorescence for lineage marker (EYFP, green) and adipocytes (FABP4, red) after conditional removal of IFT88 in FAPs 21 dpi with glycerol injection. Scale bar is 50 μm.

(D) Quantifications of the percentage of EYFP-expressing FAPs at 5 dpi (n=4–5 per genotype) and 21 dpi (n=5–6 per genotype) with glycerol injection. All data are represented as mean ± SEM. See also Figure S5.

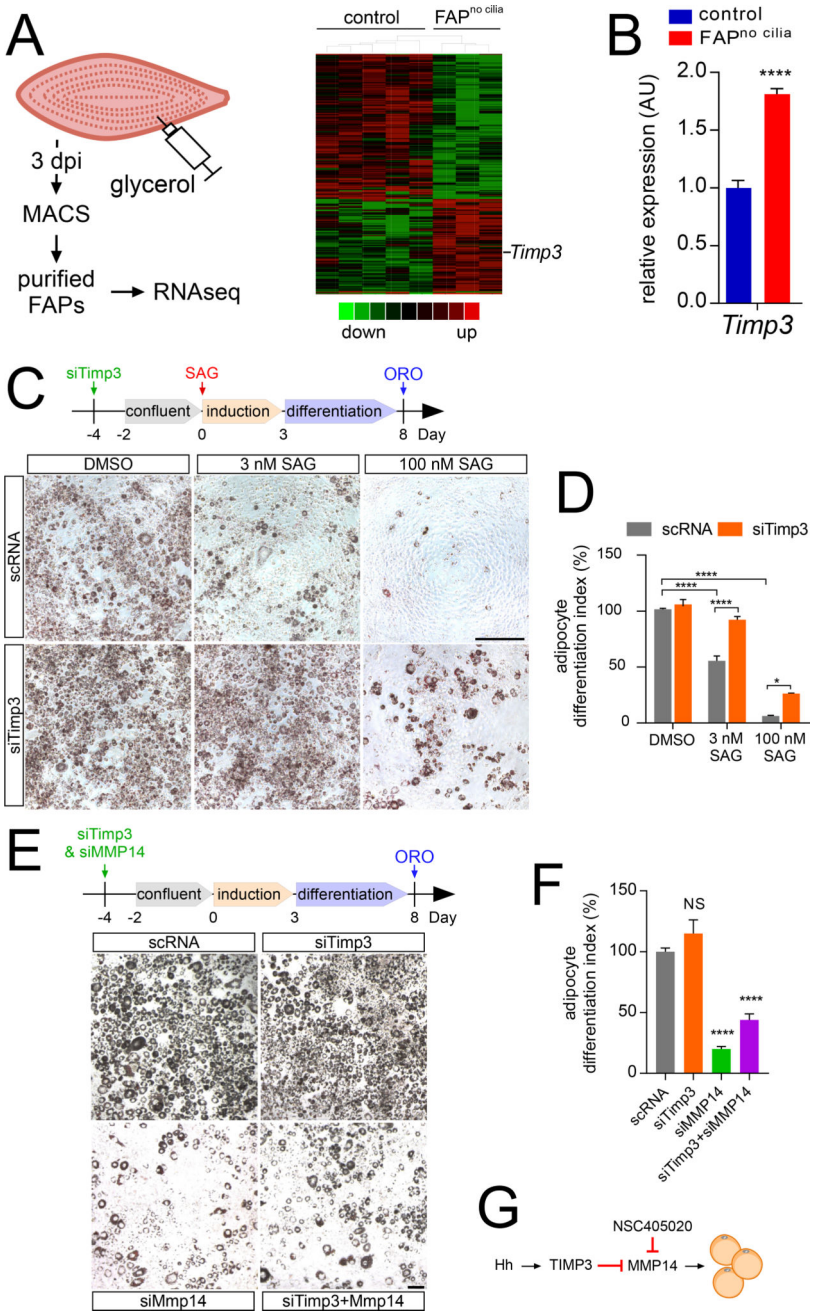

Figure 6. Hh signaling represses adipogenesis via induction of TIMP3

(A) Graphical representation (heatmap) of RNAseq transcriptional profiling of MACS-purified FAPs at 3 dpi (n=12–14 per genotype per sample).

(B) RT-qPCR analysis of MACS-purified FAPs with and without IFT88 at 3 dpi (n=5–6 per genotype) for *Timp3*.

(C) Oil red O staining of 3T3-L1 cells 8 days after adipocyte differentiation in the presence or absence of either 3 or 100 nM SAG. 4 days prior to induction, 3T3-L1 cells were transfected with a scramble siRNA control (scRNA) or siRNA against *Timp3* (siTimp3). Scale bar is 500 μm.

(D) Quantifications of the percentage of Oil Red O occupied area. The scRNA control treated with DMSO was set to 100% and all data normalized to it (n=8 per condition).
(E) 3T3-L1 cells were transfected with scRNA, siTimp3 and/or siMmp14, stimulated to differentiate as adipocytes 4 days after transfection, and stained for Oil Red O 8 days after adipocyte induction. Scale bar is 100 μm.
(F) Quantifications of the percentage of Oil Red O occupied area (n=6 per condition). All data are represented as mean ± SEM.
(G) Model of how TIMP3 inhibits adipogenesis by blocking MMP14 function. See also Figure S6.

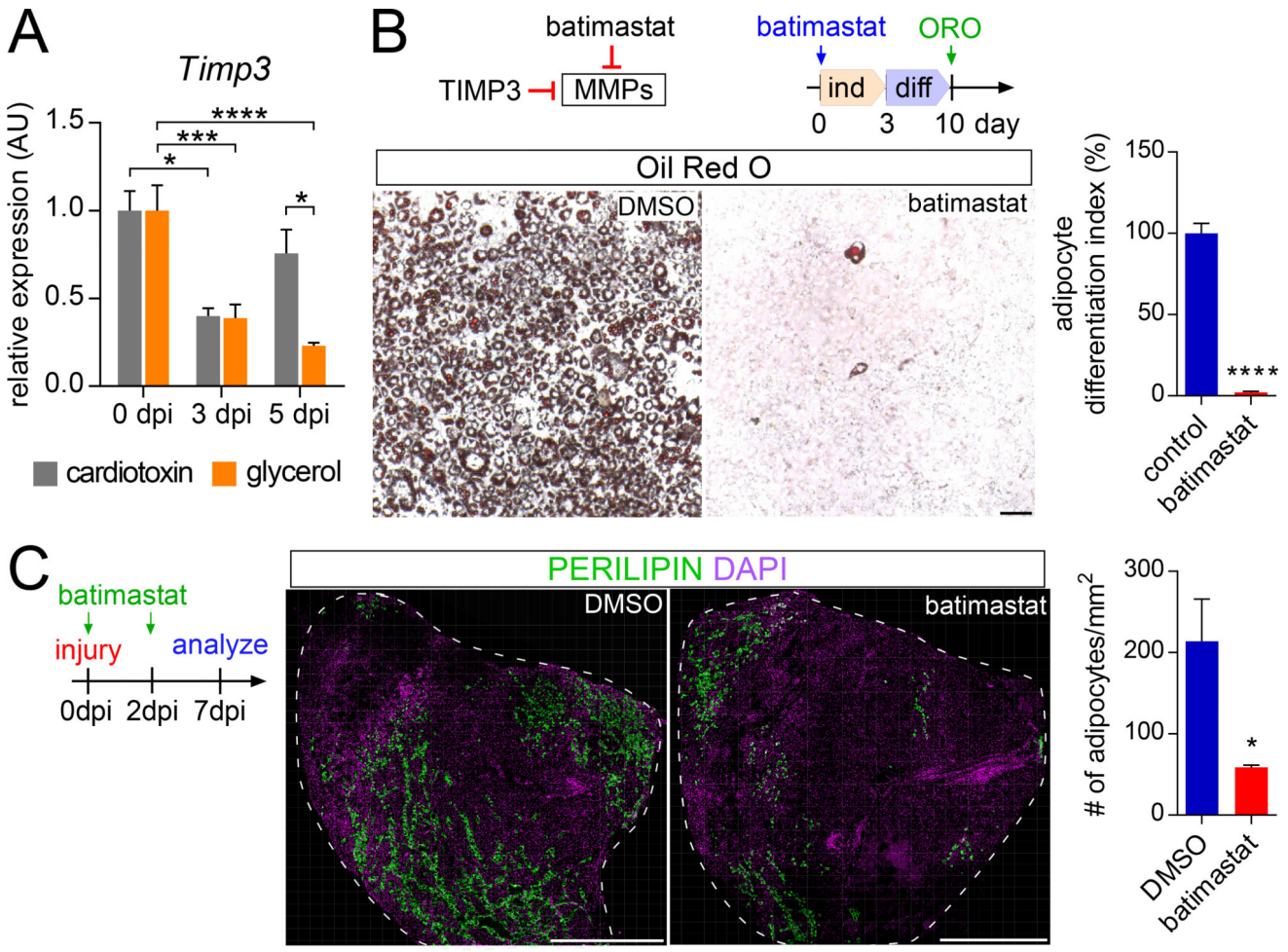

Figure 7. TIMP3 activity restrains intramuscular fat formation

(A) *Timp3* RT-qPCR analysis of RNA isolated from whole tibialis anterior muscle without injury or 3 and 5 dpi with injection of cardiotoxin (gray) or glycerol (orange) (n=4 per time point and injury).

(B) Oil Red O staining of 3T3-L1 cells treated with DMSO or batimastat, a pharmacological mimic of TIMP3 function, 10 days after the induction of adipocyte differentiation. Scale bar is 100 μm. (right side) Quantifications of Oil Red O occupied area with scale set to 100% for DMSO control (n=6 for both conditions).

(C) Immunofluorescence of adipocytes (PERILIPIN, green) 7 dpi with glycerol injection in wild type mice injected with either DMSO or batimastat at day 0 and day 2. Scale bar is 1 mm. Right: Quantifications of number of adipocytes per $1mm^2$ of injured area 7 dpi (n= 4–6 per treatment group). All data are represented as mean ± SEM.